Detecting Coherent Phonon Wave Effects in Superlattices Using Time-Domain Thermoreflectance

by

Maria N. Luckyanova

Submitted to the Department of Mechanical Engineering
in partial fulfillment of the requirements for the degree of

Master of Science in Mechanical Engineering

at the

MASSACHUSETTS INSTITUTE OF TECHNOLOGY

February 2012

Author .....
Department of Mechanical Engineering
January 20, 2012

Certified by .....
Gang Chen
Carl Richard Soderberg Professor of Power Engineering
Thesis Supervisor

Accepted by .....
David E. Hardt
Chairman, Department Committee on Graduate Theses

Detecting Coherent Phonon Wave Effects in Superlattices Using Time-Domain Thermoreflectance

by

Maria N. Luckyanova

Submitted to the Department of Mechanical Engineering
on January 20, 2012, in partial fulfillment of the
requirements for the degree of
Master of Science in Mechanical Engineering

Abstract

Superlattices (SLs), structures consisting of periodic layers of thin films of several angstroms to tens of nanometers thick, have unique electrical and thermal properties that make them well suited for applications in optoelectronics and as fundamental learning tools in the realm of thermoelectrics. One unique characteristic of SLs is their low thermal conductivity compared to a bulk material with the same molecular composition. This property has given rise to extensive theoretical and experimental investigations regarding thermal transport through SLs. The different thermal transport characteristics have been studied in the context of various transport regimes. In this thesis, an experimental investigation of thermal transport in the coherent regime through a SL is presented.

The trend in thermal conductivity that can be expected if such coherent wave effects exist is dervied from the Landauer-Büttiker formalism, which treats energy transport as a transmission process. The frequency-dependent transmission probability for phonons through the SL is found via an application of the transfer matrix method (TMM). The calculations show that the integral effect of the buildup of phonon stopbands in the SL is minimal. Thus, if coherent wave effects are present, the conductance of the SL is nearly constant as the number of periods is increased, and the thermal conductivity, which is the product of the conductance and the total thickness of the SL, increases linearly with number of periods.

To test the predictions, five GaAs/AlAs SLs with one, three, five, seven, and nine periods of one layer of GaAs of 12 nm thickness, and one layer of AlAs of 12 nm thickness are grown using MOCVD. The thermal conductivities of the SLs are measured using a transient thermoreflectance (TTR) technique at temperatures ranging from 30K to 300K. The results are the first-ever experimental evidence for the presence of coherent wave effects in heat transport through SLs.

Thesis Supervisor: Gang Chen
Title: Carl Richard Soderberg Professor of Power Engineering

Acknowledgments

This thesis has been three and a half years in the making on top of four years spent as an undergrad at MIT. As a certain culmination of years of work, there are so many people I would like to thank and so many reasons to thank them that I could write an entirely separate thesis on the topic. To save trees, I'll keep the list short, but its mere completion will serve as a reminder to me for the rest of my life of how many people and institutions have helped me accomplish what I've accomplished and how lucky I am to have had all of them in the folds of my life.

First, I would like to acknowledge my advisor, Prof. Gang Chen. He took me into his auspices in my second year of graduate school, when I had lost my bearings and my forward progress felt stalled. He believed in me and challenged me to believe in myself. Despite his busy schedule, he always makes time for his students and always strives to improve the opportunities available to us. He has gone far above and far beyond my expectations of an advisor, and I look forward to working towards my Ph.D. with him. I also thank Gang for welcoming me into the Nanoengineering Group.

As a member of the group, I was fortunate to be surrounded by some of the nicest and most hospitable people at MIT, people whose enthusiasm for science and exploration was contagious and a welcome sign that I was in the right place. I would particularly like to thank Austin Minnich, Kimberlee Collins, Jivtesh Garg, Keivan Esfarjani, Prof. Aaron Schmidt of BU, and Alex Maznev and Jeremy Johnson of Prof. Keith Nelson's group in the chemistry department. Without their invaluable help and support this project would have turned out far less successfully and been much less fun to do. I am gratfeul to them for their time, guidance, and friendship.

I am very thankful to the NSF for supporting my research here as part of their Graduate Fellowship Program.

My experience at MIT has been made far richer by the terrific friends I've made here. Though they have scattered across the globe, they each—Melis, Elysa, Jess, and Tess—remain an indelible part of me. I would especially like to thank my teammate

Billy Putnam. Billy pushes me when I'm lazy and believes in me unconditionally. With him in my life, winter is warmer, rainy days are brighter, and living is livelier.

Finally, I am thankful to my wonderful parents and my amazing sister. My parents moved to this country with nothing but I never wanted for anything. They instilled a deep respect for education and achievement that has persistently driven me while I've been at MIT. They also gave me my very best friend, my sister Natalia. Her good cheer, hospitality, and love for me have always been unflappable, and knowing that she'll be there to support me no matter what has given me confidence through any endeavor. Everyone's life would be better and fuller if they had a sister like mine.

Contents

List of Figures

List of Tables

Chapter 1

Introduction

As devices of all types—from optoelectronics to power generation—continue getting smaller, controlling the movement of heat within them will become increasingly important. Moore's law has thus far been accurate, predicting that the number of transistors that can fit on an integrated circuit device doubles every two years, with the potential of computing devices continually increasing [1]. One unintended consequence of high density integrated circuits is the production of a great deal of excess heat that must be carried away from these devices at an ever increasing rate [2]. As a result, it has become increasingly important to determine which nanoscale structures and devices are best at carrying away heat using both empirical and theoretical methods. Many of these efforts are aimed at gaining a fundamental understanding of nanoscale heat transfer so as to better focus the designs of these structures. This thesis aims to contribute to the understanding of heat transport at the nanoscale via a close and unique experimental investigation of superlattices (SLs), structures that have received a great deal of attention during the last quarter century.

Superlattices were first considered by L. Esaki and R. Tsu in 1970 [3]. Superlattices (SLs) are periodic stacks of thin films each with a thickness that can be anywhere from several angstroms to tens of nanometers thick. The thickness of the entire SL structure can range from anywhere between several hundreds of nanometers to tens of microns thick, depending on its application (Fig. 1-1). Superlattices can be made from a wide variety of materials including metals [4, 5, 6], semiconductors [7, 8],

dielectrics [9, 10], thermoelectrics [11, 12, 13], quantum dots [14], and even liquids [15, 16]. SLs were originally time-consuming and expensive to fabricate, requiring lengthy and resource-consuming epitaxial processes. Recently, the rapid development of faster and cheaper nanofabrication techniques that have maintained the high quality of epitaxial growth systems, has driven down the cost of production, increasing the availability of SLs and broadening their potential applications [17, 18].

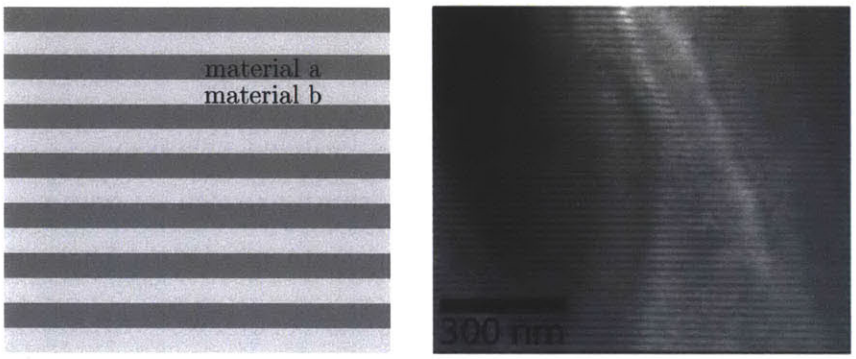

(a) (b)

Figure 1-1: (a) Schematic representation of a superlattice (SL), a periodic nanostructure consisting of alternating layers of thin films on the order of 1-10 nm thick. (b) An X-TEM image of a GaAs/AlAs SL fabricated using MOCVD. The sample was fabricated by A. Jandl of Prof. Gene Fitzgerald's group at MIT.

1.1 Superlattice Applications

Superlattices have found applications in a number of areas, including optoelectronic devices like quantum cascade lasers (QCLs), which employ SLs as the lasing medium [19, 20], and power-generation devices such as thermoelectric (TE) modules [12, 13].

Quantum cascade lasers (QCLs) are one of the most important sources of coherent light in the mid- to far- infrared and THz regimes. These light sources take advantage of the electronic structure of SLs to generate light. Alternating thin films act as

quantum wells with discrete energy subbands. As an electron moves through the SL, it undergoes inter-subband transitions within these quantum wells, and then tunnels through the next thin film which acts as a barrier region. It emerges from the barrier into another quantum well where it undergoes another identical intersubband transition, thus creating a cascade of coherent photons [20]. These intersubband transitions are shown in Fig. 1-2. The first QCL contained an InGaAs/InAlAs SL as this active region [19]. Since then a number of other semiconductor systems have been used. As a coherent mid- to far- infrared or THz light source, QCLs have applications that range from medical to military technologies [20].

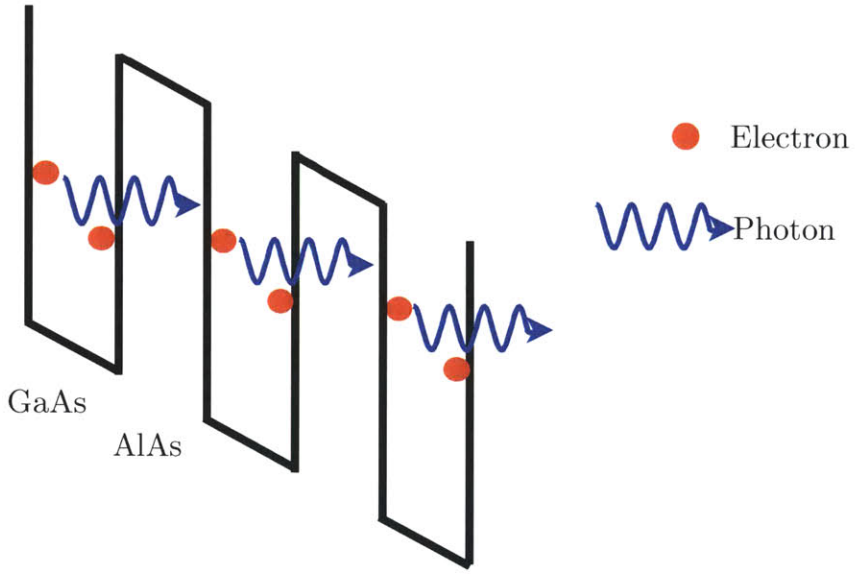

Figure 1-2: Intersubband transition in the SL active region of a QCL.

In the realm of thermoelectrics (TE), SLs are attractive because of their inherent thermal and electrical properties [21, 22, 23]. They serve as a fundamental learning tool for the design of TE materials and structures. This is because the standard by which TE materials are measured, the figure of merit ZT, is proportional to the electrical conductivity, σ, of a material and inversely proportional to the thermal conductivity, k, and is given by the following equation, where S is the Seebeck coefficient,

$$ZT = \frac{S^2\sigma}{k}T. \tag{1.1}$$

Thus, a material with high electrical conductivity but low thermal conductivity is desirable. In most metals, however, thermal conductivity and electrical conductivity are inherently linked, such that materials with high electrical conductivities have high thermal conductivities, and vice versa. The ZT for bulk materials typically is on the order of 1 or less. On the other hand, SLs can be fabricated to have lower thermal conductivities than their bulk counterparts without sacrificing electrical conductivity [24, 25]. The SL has therefore emerged as a promising way to decouple thermal and electrical conductivities, theoretically yielding higher ZTs.

Several groups have taken advantage of these properties of SLs to improve the performance of TE devices. In 2001, a group claiming to have produced a TE element with a ZT of 2.4 based on Bi_2Te_3/Sb_2Te_3 SLs reported that the enhancement was primarily due to the greatly decreased phonon transport through the SLs [13]. In 2009, Chowdhury and colleagues demonstrated a chip-scale cooling device employing SLs in the TE element that was the first of its kind (Fig. 1-3). Previous attempts at this scale of TE-based cooling devices ran into structural limitations, but the group demonstrated that the use of Bi_2Te_3 based SLs which are fully integrated into the supporting electronics can achieve adequate cooling rates when devices are operating with high power fluxes [12, 26].

Other applications of SLs have also been proposed recently, including an acoustic rectifier that uses a SL as a key component of the device. By coupling a SL with a thin layer of ultrasound contrast agent microbubble suspension, commonly used to help visualize the results of ultrasound scans, acoustic energy rectifying ratios on the order of 10^4 were achieved [15, 16].

Due to their great potential in a number of applications, many studies, both theoretical and experimental, have been conducted to understand the interesting electrical, optical, and thermal properties of SLs. These studies contribute to the large pool of knowledge that provides insight into various aspects of SL behaviors. Among these studies, it has been demonstrated that SLs can be designed with thermal conductivities well below that of bulk materials with similar chemical compositions. While a number of mechanisms have been proposed to shed light on these findings, none

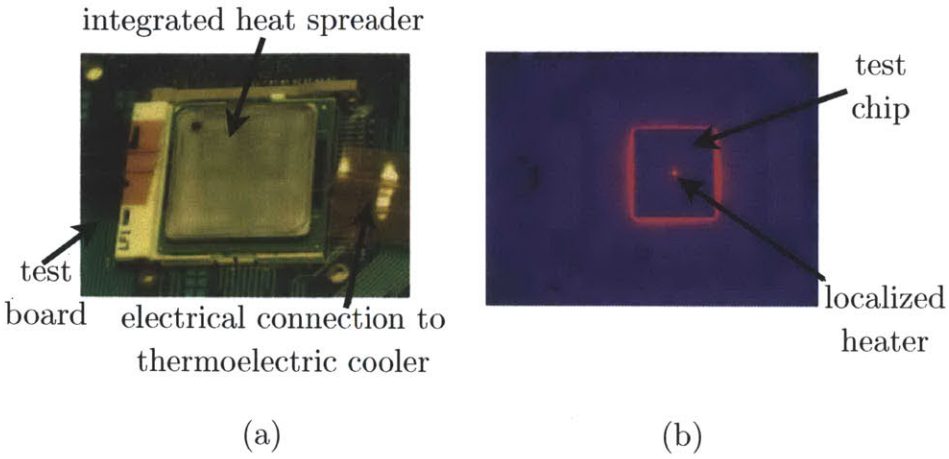

Figure 1-3: (a) Photograph of the experimental SL-based cooling device. The electrical connections power the TE cooler located under the heat spreader. The test board contains hardware to read the temperature of the chip. (b) An infrared image showing the distribution of the heat load during chip operation. Figure reproduced from [12].

can single-handedly explain them. This thesis is concerned with advancing the fundamental knowledge and understanding of the heat transport properties of SLs by studying the effect that coherent phonon transport has on the thermal conductivity of SLs.

1.2 Models for Heat Transport through SLs

A number of mechanisms have been proposed to explain the reduced thermal conductivity of SLs compared to their bulk counterparts. In order to understand these mechanisms, it is first necessary to understand the different regimes in which heat transport may happen in a SL. This section consists of a summary of the relevant transport regimes, diffusive and ballistic. Within the ballistic regime, coherent and incoherent transport is discussed. Finally, an overview of the mechanisms that have been proposed to explain thermal transport within SLs is presented.

Which transport regime is relevant to a particular explanation depends on the

mean free path (MFP), Λ, of a phonon within the material or structure. The MFP is the average distance over which a phonon can travel without incurring a scattering event. It is dependent both on the material properties as well as the temperature of the material. Internal scattering within a bulk material may involve phonon-phonon scattering or a phonon scattering off of an impurity. Assuming the material lacks impurities, the phonon-phonon processes dominate over internal scattering. At higher temperatures, a greater phonon population exists, leading to more phonon-phonon scattering events [27]. Thus, at higher temperatures MFPs are short, on the order of hundreds of nm. At low temperatures, this MFP can be much longer [28, 29]. For example, the 50% MFP of GaAs at room temperature, 300K, is 147 nm. In other words, the phonons whose MFP is less than 147 nm account for half of the thermal conductivity of GaAs at this temperature. At 100K, this 50% MFP is 900 nm [30].

Diffusive transport occurs when the characteristic length scale is much larger than the MFP, $d >> \Lambda$. In the diffusive regime, the phonons go through several scattering processes, attaining a local equilibrium, or a definable temperature at every point within the structure. Transport that occurs at a scale shorter than the MFP, $d \sim \Lambda$, is either ballistic or quasi-ballistic. In this regime, phonons have largely not undergone scattering events and a local temperature cannot be defined. In the quasi-ballistic or ballistic regime, local thermal equilibrium does not exist. At room temperature, layers of GaAs whose thickness is much greater than 147 nm behave like bulk GaAs and transport within them can be treated as diffusive. Indeed, films with relatively large thicknesses have thermal conductivities that are unchanged compared to bulk thermal conductivities [31]. Transport through layers whose thickness is on the order of 147 nm is quasi-ballistic, and transport through layers that are much thinner than 147 nm is mostly ballistic.

The addition of impurities such as crystal defects, crystal boundaries, or interfaces artificially adds scatterers where they otherwise would not exist. These impurities reduce the effective MFPs of a material [32, 33]. The constituent layers of a SL are usually thinner than the MFP of the materials. As a result, there is very little scattering within the layers comprising the SL themselves and the phonons travel bal-

istically through them. However, the interfaces between the layers scatter phonons. The phonons may either be scattered coherently such that their phase information is preserved or incoherently, such that all phase information is lost. When the scattering is incoherent, the presence of the interfaces effectively reduces the MFP of phonons within the structure. Thus, again, a quasi-local thermal equilibrium can be defined within the structure when one looks at a region thicker than one layer. This is referred to as the coarse-grained model and is depicted in Fig. 1-4(a). In this regime, the SL behaves like a bulk material with a MFP on the order of a layer thickness. When the phonons scatter coherently off the interface, wave mechanics becomes relevant. In this regime the SL behaves like an entirely new material with a unique crystollagraphic structure defined by the presence of periodic interfaces. This new 1-D periodic structure has its own dispersion relation and relevant transport properties.

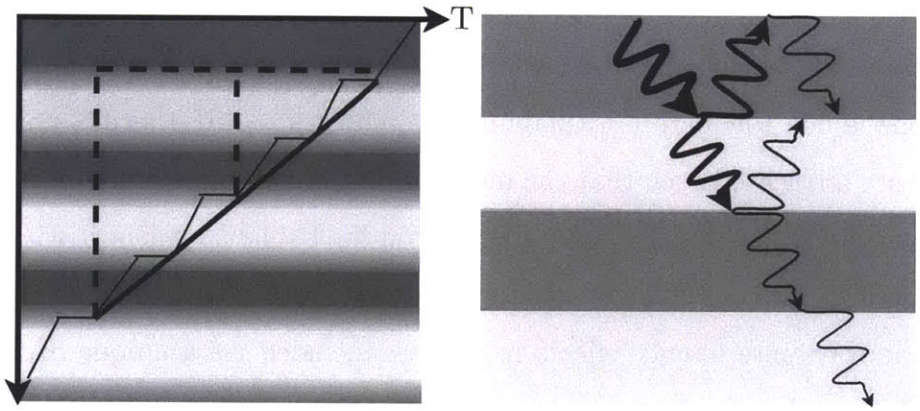

Figure 1-4: (a) Diffusive model of heat transport through a SL, with a linear temperature drop within each layer due to internal diffuse scattering, and a thermal resistance at every interface. If this jagged temperature profile is coarse grained, a linear temperature profile through the SL emerges, corresponding to an effective thermal conductivity. This picture is accurate in the limit where the SL layer thicknesses are greater than the phonon MFPs. (b) Phonon interference effects from multiple interfaces lead to a modified dispersion relation which modifies the heat transport through the SL through a variety of effects, such as decreased phonon group velocities or higher scattering rates.

Theories that treat heat transport through SLs as ballistic and incoherent contend that the reduction in thermal conductivity of SLs compared to bulk materials with the same chemical composition is due primarily to diffuse scattering at the interfaces between two materials. This diffuse scattering can be caused by a number of mechanisms, including atomistic mixing and diffusion at the interfaces, strain and dislocations caused by the two materials having different lattice constants, rough interfaces stemming from an imperfect growth process, or anything else that might cause a loss of coherence for phonons that impinge upon the interface. It has been shown that roughness that could lead to diffuse interface scattering is present even under the best growth conditions [34]. Interface scattering, both diffuse and ballistic, creates a specific thermal resistance, often referred to as the Kapitza resistance, that leads to a temperature drop from one side of the interface to the other [35, 36]. This thermal interface resistance has been observed at the interfaces of every dissimilar materials system, and a fundamental understanding of how it arises is also lacking [37].

However, experiments have shown that interface resistance due to diffuse scattering alone is not adequate in explaining the reduction in SL thermal conductivity. Most SLs are fabricated such that the individual layer thicknesses are on the order of or less than phonon MFPs. In this configuration the ballistic transport within the SL layers as well as any possible coherent wave contributions have to be considered. In general, the wave interference effects in SLs are included via a unique SL dispersion relation, first studied by Narayanamurti et al., who showed that interference effects due to the periodic presence of interfaces (Fig. 1-4(b)) lead to a modified dispersion relation. The dispersion relation in a periodic solid, such as a crystal or a SL, dictates how phonons of specific energies will contribute to energy transfer in the material, and is highly dependent on the unique chemical composition of the material as well as the periodicity of the material. A crystal typically has a periodicity on the order of several angstroms. SLs, on the other hand, have periodicities on the order of one to ten nm, and thus have a greatly modified dispersion relation from what one typically observes in a crystalline material [38]. Since the periodicity of the SL is much greater

than a regular crystal, the size of the brillouin zone (BZ), which increases inversely with the size of the repeated period in a structure, is greatly reduced compared to the BZ in a bulk crystal, leading to zone folding [39, 40, 41]. Conceptually, zone-folding leads to a number of conclusions regarding the phonon transport through the SL.

One conclusion is that the group velocity of phonons traveling with wavevectors near the edge of the BZ approaches zero. Thus, phonons that in bulk materials would contribute to heat transfer are stymied by a reduced group velocity [41, 42]. Although this effect can partially account for a reduction in the overall thermal conductivity in GaAs/AlAs SLs in a lattice dynamics model of a SL, overall agreement with experimental values is poor. It is also clear that just one consequence of the unique SL microstructure is not sufficient to explain the modified thermal transport properties [43].

A modified crystallographic structure and dispersion relation leads to different scattering rates than would be seen in the bulk constituent materials, some of which could increase the thermal conductivity of SLs and others of which could decrease it. For example, a smaller BZ with a flattened dispersion reduces bulk Umklapp scattering rates, thus increasing the thermal conductivity, an effect that competes with the lower phonon group velocities [44]. Other studies, however, have shown that the rates of mini-Umkkapp processes, which result from the mini-zones created by zone-folding, actually increase, thereby decreasing overall thermal conductivity [45]. Aside from these competing effects due to scattering within the modified crystal, there is also a reduction in thermal conductivity due to the mass mismatch between different layers. This effect generally reduces SL thermal conductivity [46].

Several studies have presented theories and procedures that include multiple potential SL effects in order to explain their reduced thermal conductivity. The techniques used to model SL thermal behavior have included lattice dynamics (LD) [42, 47, 48], the Boltzmann Transport equation (BTE) [49, 50], and molecular dynamics (MD) simulations [51], among others. These theoretical investigations of the thermal behavior of SLs have yielded a great breadth of information. Many of the mechanisms described in the theoretical work have competing effects on the overall

thermal properties of the SLs, are heavily material dependent, and also vary depending on the geometry of the SL. A great deal of experimental work has been carried out to further enhance the understanding of SL behavior and to complement the theoretical investigations.

1.3 Previous Experimental Investigations

A study from 1979 supported the theory that wave mechanics plays some role in thermal transport in a SL. The group used a transfer matrix method (TMM) to determine the theoretical transmission of phonons in the (111) direction of a GaAs/AlGaAs SL. Using superconducting tunnel junctions as phonon generators and detectors, they were able to detect the attenuation of phonons in the frequency bands expected from wave mechanics calculations [39]. Similarly, in 1986, photoluminescence experiments showed electric carrier localization in GaAs/GaAlAs SLs. Random variation of the thicknesses of the SL layers changed the efficiency with which photo-excited electrons traveled through the SL. As the disorder in the layer structure increased, so too did the inhibition of carrier transport [52].

Knowing the thermal transport properties of SLs is fundamental to designing them for optoelectronic or energy harvesting purposes. Thus, many experimental studies have been performed to determine the thermal transport properties of SLs. These studies have largely focused on determining the thermal conductivity of SLs with varying period thicknesses. One of the first such studies was performed in 1987 by T. Yao, who used ac calorimetry to study the in-plane thermal conductivity of GaAs/AlAs SLs at room temperature. Yao found that the thermal conductivity of the SL along the film-plane direction was larger than that of an alloy with the same molecular composition, and attributed this effect to the suppression of alloy scattering. In addition, he found that there was an overall increase in SL thermal conductivity with increasing SL period thickness. Yao's results were among the first experimental studies of thermal transport properties of SLs [53].

The first experimental investigation of cross-plane thermal conductivity of SLs was

conducted by G. Chen and colleagues. Although SLs can be grown over large areas, their thicknesses are usually limited to several microns. As a result, experimental techniques that require contact with the sample, such as ac calorimetry, introduce a great deal of error because the contact resistance can be on the order of or larger than the SL thermal resistance. Chen *et al.* used a non-invasive optical technique to measure the thermal diffusivity of GaAs/AlAs SLs. They provided an important benchmark for future theoretical and experimental studies, as they showed that SL cross-plane thermal conductivity was less than its bulk counterpart [8].

Similarly, subsequent studies used a range of different experimental techniques to show that SLs mostly have larger thermal conductivities than alloys of the same molecular composition, and an increasing SL thermal conductivity with increasing SL period thickness. At very small periods, the SL conductivity approaches the alloy limit and in some cases is even lower than the alloy value [8, 54, 55]. These studies also looked at the temperature dependence of the SL thermal conductivity. Since different scattering mechanisms have different temperature-dependent behaviors, studies of thermal conductivity with temperature lend insight into the dominant scattering mechanisms for certain SLs. Different material systems were found to behave differently with temperature. Below a critical temperature, GaAs/AlAs thermal conductivity increases with increasing temperature, contrary to the behavior of a bulk single crystal material. However, at higher temperatures (>100 K), the thermal conductivity appears to decrease with increasing temperature, suggesting that at these temperature ranges, phonon-phonon scattering is the dominant mechanism behind thermal conductivity reduction in the SLs used for the studies [54, 56, 57]. The thermal conductivities of Si/SiGe and SiGe/SiGe SLs, on the other hand, increase with increasing temperature [55, 58]. This behavior is characteristic of materials where defect scattering dominates thermal behavior.

Many of the experimental and theoretical investigations carried out thus far into the thermal properties of SLs have shown that incoherent transport plays an important role in SL thermal behavior. However, these studies have left the door open to investigating the role that coherent transport plays in this thermal behavior. In this

thesis, an experimental investigation into the role of coherent transport is presented.

1.4 Organization of this Thesis

The experimental investigations performed on SLs thus far have varied the period length and the temperature and determined the thermal conductivity dependence of the SLs on these properties. We have approached the problem from a different perspective. Rather than vary the width of the period, we have varied the number of periods in our samples in order to detect coherent wave effects in SLs. By varying the number of periods in the structure, we can add to the growing understanding of the properties of SLs. The number of periods in our SLs vary from one to nine. A non-invasive, optical pump-and-probe technique is used to measure the through plane thermal conductivity of five MOCVD-grown GaAs/AlAs SLs ranging from one period to nine periods thick.

In Chapter 2, the predicted trend of the thermal conductivity of the SLs when coherent phonon transport dominates is presented. The calculations are based on the Landauer-Büttiker formalism which treats energy transport as a transmission process. The most important quantity necessary in applying this formalism to the problem of determining thermal transport properties is the transmission probability. This probability is found by applying the transfer matrix method to phonons traveling through the SL. A thorough quantitative calculation of the thermal conductivity using the Landauer-Büttiker formalism would involve a great deal of complexity and can require tremendous computing power. Due to the experimental nature of this thesis, simplifying assumptions are made and the calculations presented herein represent only the expected trend of the thermal conductivity of SLs.

Chapter 3 outlines the transient thermoreflectance (TTR) experimental technique used to study the thermal transport properties of the SLs as well as the process used to grow them, molecular organic chemical vapor deposition (MOCVD). The thermal conductivities of the SLs are measured at a wide range of temperatures. The resulting thermal conductivities as well as other relevant data are presented in chapter 4.

Finally, Chapter 5 delves into the potential future directions in which this study can continue. This experiment has, for the first time to our knowledge, experimentally demonstrated the presence of coherent wave effects in SLs. This result greatly increases the knowledge that exists regarding heat transport through SLs and could provide a great checkpoint for theoretical investigations into SL properties.

Chapter 2

Theory and Calculations

In this chapter, the modeling and calculations used to derive the expected behavior of the SL thermal transport properties based on a coherent transport picture are explained. The Landauer-Büttiker formalism is applied to the limit where there is no internal scattering and all transport is coherent. The Landauer-Büttiker formalism treats energy transfer as a transmission process [59, 60, 61], a treatment that is well suited to coherent wave transport because wave mechanics can be used to simply find the transmission coefficient. The TMM takes into account the multiple phonon reflections that occur at interfaces, leading to the buildup of an interference pattern, as suggested by Fig. 2-1. The first TMM calculation to determine the thermal conductance through SLs was performed by G. Chen [62, 63] and several later studies replicated the procedure [64, 65, 66]. The remaining elements of the Landauer-Büttiker formalism are derived from the dispersion relations of AlAs and GaAs. The trend of thermal properties due to coherent transport is compared to predicted thermal properties based on a completely diffusive picture of transport, where the fully classical limit is assumed.

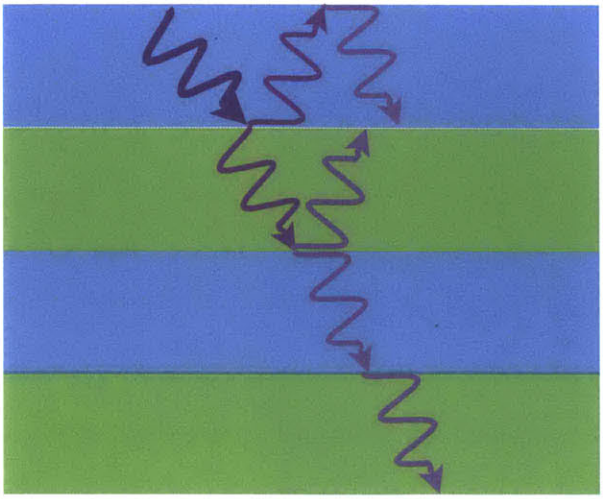

Figure 2-1: In the coherent picture of transport, when a phonon wave impinges on an interface, it can either be reflected or transmitted with its phase information preserved. The preservation of this phase information means that interference effects could be calculated within the SL, and the overall transmission of thermal energy depends on the transmittance of each individual carrier through the SL.

2.1 Landauer-Büttiker Formalism for Coherent Transport

The thermal conductance, K, of a structure relates the heat flux q through the structure to the temperature difference across it ΔT,

$$K = \frac{q}{\Delta T}. \tag{2.1}$$

The Landauer-Büttiker formalism treats this flux as a transmission process. If the energy contained by a carrier, in this case a phonon, and its speed are given and the transmission probability of the phonon is known, the heat flux due to this phonon can be found. Similarly, given the heat flux through and the temperature difference across the structure, the thermal conductance is known. Thus, the thermal conductance depends upon the speed of the impinging phonons, which is given by the phonon group velocity, v_g, the heat energy carried by these phonons, which is described by

the frequency-dependent heat capacity, C, and the probability of propagation for the phonon, or the transmission coefficient, τ

$$K = \sum_p \int_0^\omega \tau_{\omega,eff} v_{g,ave} C_{ave} \, d\omega. \tag{2.2}$$

The thermal conductance, however, is difficult to measure. The thermal conductivity is the measurable quantity, so the trend we ultimately desire to calculate is that of thermal conductivity k, the product of the characteristic length of the structure, l, and its conductance,

$$k = lK. \tag{2.3}$$

Both of the material-dependent quantities necessary for determining the thermal conductance—the heat capacity and the group velocity—are found from the phonon dispersion relation. The phonon group velocity and the heat capacity in this formulation of the thermal conductance are properties of the phonon source, which in this experimental setup is the optical-thermal metal transducer layer of Al, not the SL. In this thesis, we are interested in finding a representative trend for the behavior of the SL as a function of the number of layers. Thus, a number of approximations and assumptions are made to simplify the necessary calculation.

We are interested in determining a trend, thus we use the average frequency-dependent heat capacities and group velocities of GaAs and AlAs. Using these materials rather than Al is advantageous because the same wavevectors that appear in the transmission calculations will appear in the group velocity and heat capacity calculations. The trend should be the same as if Al had been used in determining these quantities, though the absolute magnitude of the solution will be quite different.

The Γ to X direction in the dispersion relation is chosen for determining the frequency-dependent heat capacities and phonon group velocities of AlAs and GaAs and the other directions are excluded from the calculation. Additionally, only acoustic phonons are considered because these, rather than the optical phonons, play a dominant role in heat transport because of their much larger group velocities. Optical

phonons do, however, play an important role in phonon-phonon scattering processes with acoustic phonons [67]. However, since internal scattering, under which category phonon-phonon scattering falls, is neglected in this analysis due to the small size of the constituent thin films, excluding optical phonons is a good approximation.

A polynomial fit is made to the Γ to X direction of the phonon dispersion relations of GaAs and AlAs (Fig. 2-2) [40, 68]. The size of this part of the brillouin zone is approximately equal for AlAs and GaAs due to their very close lattice constants. Thus, it is possible to take the average of the frequency-dependent properties of GaAs and AlAs when implementing these quantities in the thermal conductance calculation. This is a good assumption for the heat capacity since the heat capacity is dependent on the molecular composition of the material, and the molecular composition of the SL is well known. Averaging the group velocity, though a common practice, is less accurate. Determining a phonon group velocity based on a new dispersion relation to be calculated from the modified periodicity of the SL would be more accurate but also more time consuming and calculation-intensive. As a first approximation for the general trend followed by the conductance of the SL, an average group velocity suffices.

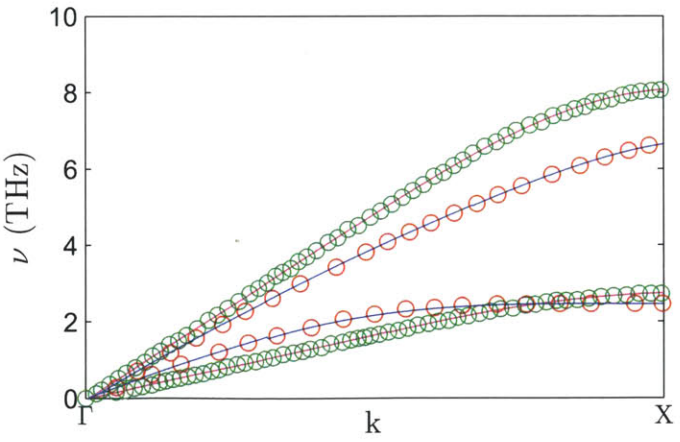

Figure 2-2: GaAs and AlAs dispersion relations. Open green circles are literature values for AlAs [40] while the solid magenta lines are combinations of several polynomial fittings to the dispersion relation of AlAs, and open red circles are literature values for GaAs [68] while the blue lines are polynomial fittings.

In the following sections, the crystal properties of GaAs and AlAs will be found based on the Γ to X direction in their dispersion relations. These properties include the phonon group velocities, the densities of states, and the heat capacities. Next, the frequency-dependent transmission coefficients of phonons traveling through the SL will be found using the TMM. The results of these calculations are used as inputs to determine the thermal conductance of the SL using the Landauer-Büttiker formalism as described above. The formalism reveals a nearly constant thermal conductance with number of periods and, subsequently, a linear increase in the thermal conductivity of the SL when coherent effects are present.

2.1.1 Phonon Group Velocity

The phonon group velocity, v_g, is determined from the slope of the dispersion relation

$$v_g = \frac{d\omega}{dk} \tag{2.4}$$

where ω is the energy carried by a certain wavevector, k. The resulting group velocities in the Γ to X direction are shown in Fig. 2-3. For the calculations presented herein, the average of the longitudinal acoustic (LA) phonon group velocities for GaAs and AlAs was used for the LA phonon group velocity in the SL, and a similar averaging was used for the transverse acoustic (TA) phonons.

2.1.2 Phonon Heat Capacity

The phonon heat capacity is defined as the change in internal energy of the material with a change in temperature at constant volume,

$$C_V \equiv \left(\frac{\partial U}{\partial T}\right)_V. \tag{2.5}$$

The heat capacity quite literally describes the capacity of the material to store energy. The total capacity is the sum of the energy that each phonon stores at thermal equilibrium. Each phonon is treated like a harmonic oscillator, with a quantized

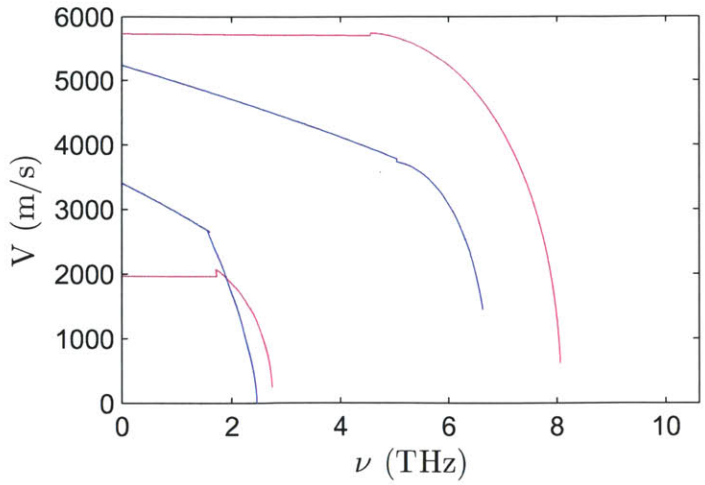

Figure 2-3: GaAs and AlAs group velocities. Pink lines are for AlAs group velocities (with the higher velocity corresponding to longitudinal acoustic (LA) phonons, blue lines are GaAs group velocities. The kinks in the group velocity curves are due to small discontinuities in the polynomial fittings of the dispersion relation. They have a negligible effect on the rest of the calculations.

energy based on wavevector and temperature. The heat capacity is found by summing the energy stored in each normal phonon mode of the solid over the number of phonons at each of these modes, a quantity called the density of states (DOS). The density of states per unit volume for a specific polarization, $D(\omega)$, is the number of states that is occupied at each energy level. It is found using the following formula

$$D(\omega) = \frac{4\pi k^2}{(2\pi)^3} \frac{dk}{d\omega}. \tag{2.6}$$

The resulting DOS is shown in Fig. 2-4.

When the distribution of phonon modes, the energy stored in each mode, and the density of states are summed over all possible modes and the three acoustic phonon polarizations—two transverse arms and one longitudinal arm—the total heat capacity is given by

$$C = k_B \sum_p \int_0^{\omega_{max}} D(\omega) \frac{(\frac{\hbar\omega}{k_B T})^2 e^{(\frac{\hbar\omega}{k_B T})}}{(e^{(\frac{\hbar\omega}{k_B T})} - 1)^2} d\omega. \tag{2.7}$$

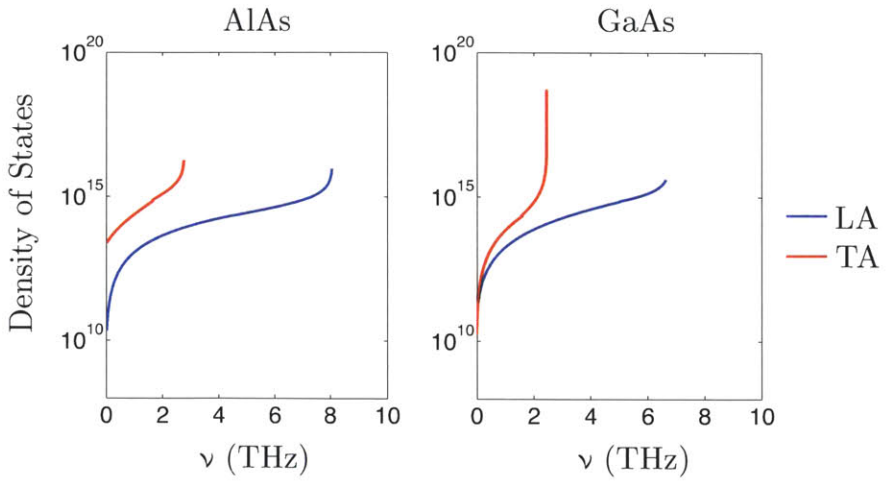

Figure 2-4: GaAs and AlAs DOS for acoustic phonons in the Γ to X direction.

The resulting heat capacity, shown in Fig. 2-5, differs from experimentally determined heat capacities because only one wavevector direction and only the acoustic branches of the phonon dispersion relation are counted. The heat capacity used in calculating the thermal conductance trend, as stated above, is the average of the heat capacities determined for GaAs and AlAs since the molecular makeup of the SLs is 50% GaAs and 50% AlAs.

2.1.3 Phonon Transmission Calculations

The transmission of phonons is determined via an application of wave mechanics. In the fully coherent picture, phonons are either specularly reflected or transmitted at an interface. Multiple reflections and transmissions within layers create destructive or constructive interference, as with light waves in a dielectric stack. The frequency-dependent phonon transmission coefficients are found using the transfer matrix method (TMM) [69]. Using the transfer matrix approach is convenient because it combines all the waves with the same wavevector within a layer into one representative wave whose net transmission is determined at each interface. The end goal of employing the TMM is to find a matrix that can relate all the waves im-

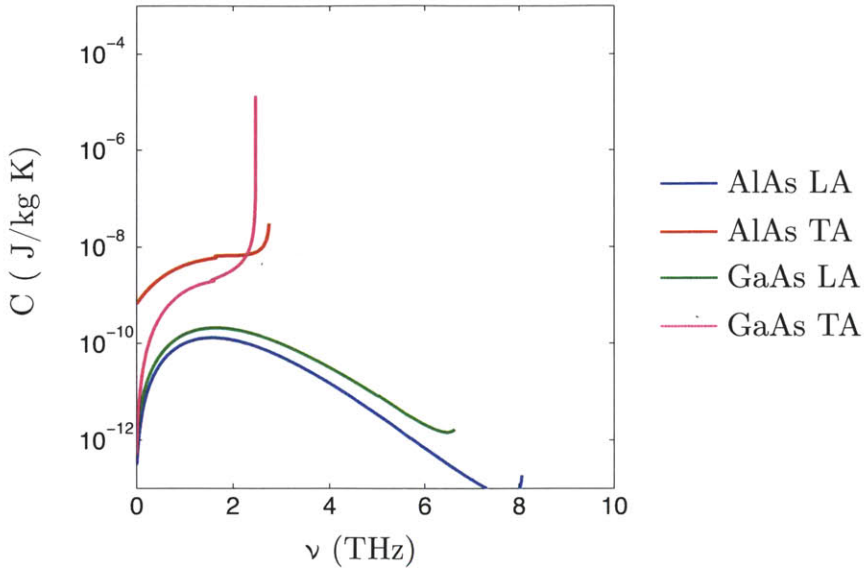

Figure 2-5: GaAs and AlAs frequency-dependent heat capacities for acoustic phonons in the Γ to X direction.

pinging on one side of the stack to all the waves transmitted through the end of the stack. With this matrix, a transmission coefficient, τ_ω, can be found for every phonon wavelength, ω.

Several simplifications are made to the phonon transmission picture to enable quicker calculations. Only normal incidence phonons are considered. This simplification yields incorrect quantitative information, but gives a general trend for what should be expected under coherent transport conditions. Since only normal incidence phonons are considered, the possibly important mode conversion and tunneling effects are not captured in this calculation [70]. Finally, to determine the very limit of thermal transport properties due to coherent phonons, no losses within the mediums or at the interface are considered.

At an interface, a phonon wave can be reflected, transmitted, or both. The magnitude of the reflection and transmission depends on the mismatch in acoustic impedance between the two media. To determine the acoustic impedance simply, we use the Debye approximation, which predicts a linear dispersion relation. Under this approximation, the acoustic impedance, Z, depends upon the density and sound

velocity in the medium and is given by

$$Z_{i,p} = \rho_i v_{i,p} \tag{2.8}$$

where the subscript i refers to the material, and the subscript p refers to the polarization of the phonon since longitudinal and transverse acoustic waves have different associated sound speeds. The reflection coefficient for a wave traveling from material i to material j at an interface is

$$R_{i,p} = \frac{Z_{i,p} - Z_{j,p}}{Z_{i,p} + Z_{j,p}} = -R_{j,p}. \tag{2.9}$$

The relationship between the reflection and transmission coefficients of acoustic waves at an interface is

$$T_{i,p} + R_{i,p} = 1. \tag{2.10}$$

Thus, the transmission coefficient of an acoustic wave traveling from medium i to medium j is found to be

$$T_{i,p} = \frac{2Z_{i,p}}{Z_{i,p} + Z_{j,p}}. \tag{2.11}$$

A scattering matrix represents an intuitive way to understand the relationship between waves on two sides of an interface and the reflection and transmission coefficients. For example, let a be a wave originating in medium i of polarization p and b be a wave originating in medium j, also with polarization p. When a travels towards medium j with magnitude a^+, it impinges upon the medium and a fraction of it, determined by $T_{i,p}$ is transmitted into medium j, while a fraction is reflected, and travels back into medium i with a magnitude a^- equal to $R_{i,p}a^+$ (Fig. 2-6). Similar analysis can be applied to a wave originating in medium j, traveling towards the same interface. In matrix format, these interactions of wave and interface are

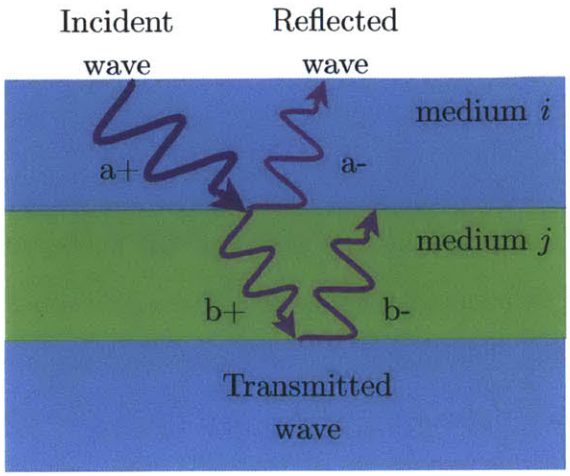

Figure 2-6: This is a diagram of the relationships between the various waves within the layers of the SL.

described with

$$\begin{bmatrix} a^- \\ b^+ \end{bmatrix} = \begin{bmatrix} R_{i,p} & T_{j,p} \\ T_{i,p} & R_{j,p} \end{bmatrix} \begin{bmatrix} a^+ \\ b^- \end{bmatrix}.$$

This scattering matrix, though intuitive, makes determining the total transmission of a wave impinging on one side of an interface to another a rather difficult task since it is necessary to keep track of waves in each medium traveling in both directions. To make the calculation of the overall transmission through a stack of multiple layers more mathematically pliable, the scattering matrix, as the above is called, is translated into a transmission matrix that relates the waves on one side of an interface to the waves on the other. Such a transmission matrix looks like

$$\begin{bmatrix} b^+ \\ b^- \end{bmatrix} = \begin{bmatrix} T_{11} & T_{12} \\ T_{21} & T_{22} \end{bmatrix} \begin{bmatrix} a^+ \\ a^- \end{bmatrix}.$$

Some simple manipulation of the elements of the scattering matrix leads to the less intuitive transmission matrix for a phonon of polarization p traveling from medium i to medium j, $\mathbf{T}_{p,i\to j}$,

$$\begin{bmatrix} b^+ \\ b^- \end{bmatrix} = \begin{bmatrix} T_i - \frac{R_i R_j}{T_j} & \frac{R_j}{T_j} \\ -\frac{R_i}{T_j} & \frac{1}{T_j} \end{bmatrix} \begin{bmatrix} a^+ \\ a^- \end{bmatrix}.$$

In order to take into account wave interference effects, it is further necessary to include a propagation matrix: a matrix that describes the sinusoidal nature of the propagation of the wave through the medium (Fig. 2-7). This propagation

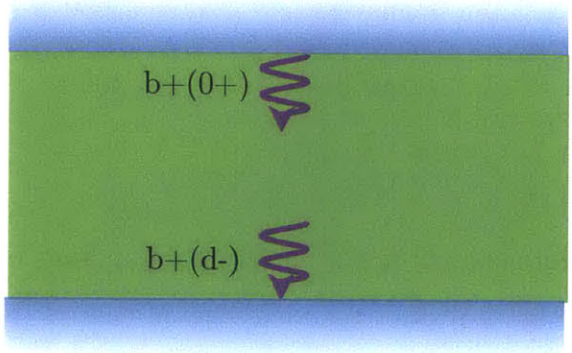

Figure 2-7: TMM wave propagation diagram.

transmission matrix, $\mathbf{T}_{p,i}$ takes into account the length of medium i through which the wave is propagating and the speed of sound through i. The forward propagating matrix is

$$\begin{bmatrix} b^+ \\ b^- \end{bmatrix} = \begin{bmatrix} exp(-i\omega d/c_0) & 0 \\ 0 & exp(i\omega d/c_0) \end{bmatrix} \begin{bmatrix} a^+ \\ a^- \end{bmatrix}.$$

The product of the transmission matrices at the interfaces and the propagation matrices within the mediums, yields an overall frequency-dependent transmission matrix, $\mathbf{T}$, that relates the phonon wave at the beginning of the SL to the end of the SL

$$\mathbf{T} = \prod \mathbf{T}_{i\to j}\mathbf{T}_{p,j}\mathbf{T}_{j\to i}\mathbf{T}_{p,i} \tag{2.12}$$

The SL materials chosen for this study are GaAs and AlAs. The properties relevant to the TMM calculation are given in Table 2.1.

Table 2.1: Material properties of GaAs and AlAs relevant to the TMM calculations. All properties are at room temperature. [71]

Material	Density, ρ [kg/m^3]	Polarization	Sound Speed, v [m/s]	Z [kg/m^2-s]
GaAs	5317.5	longitudinal	5030	26.75 *10^6
		transverse	3030	16.11 *10^6
AlAs	3730	longitudinal	5980	22.31 *10^6
		transverse	3600	13.43 *10^6

The resulting transmission coefficient both as a function of layer number and wavevector is shown in Fig. 2-8. An expanded view of part of the transmission plots is in Fig. 2-9 and gives a closer look at the development of the stopbands

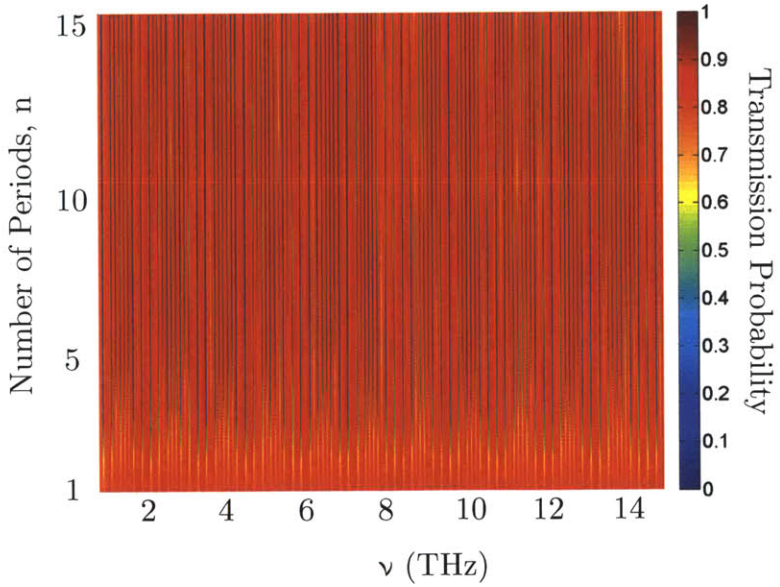

Figure 2-8: Transmission of transverse acoustic (TA) phonons normal to the SL. The color bar represents the transmission coefficient which ranges from 0 to 1.

As can be seen in Fig. 2-8, the transmission stopbands, which are the thin blue

lines in the transmission picture, represent only a very small part of the total transmission diagram. This is more readily visible in Fig. 2-9. There is a background transmission coefficient that dominates over the stopbands. This transmission coefficient is about 0.85, or the ratio of the acoustic impedances of GaAs and AlAs.

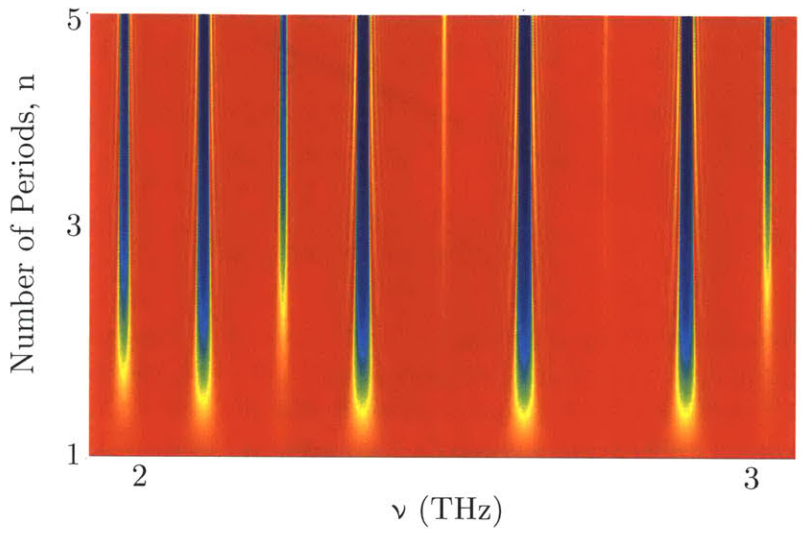

Figure 2-9: An expanded view of the transmission probability for TA phonons through the SL.

2.1.4 Superlattice Thermal Conductance

With all the necessary ingredients – SL heat capacity, phonon group velocity, and phonon transmission coefficient – the Landauer-Büttiker formalism yields the thermal conductance and its inverse, the more familiar thermal resistance, in the limit of totally coherent phonon transport through Eq. 2.2. The resulting thermal resistance is shown in Fig. 2-10.

This figure shows that, despite the buildup in stopbands, the effect on the resistance of the changing transmission coefficient over a growing number of periods is, in fact, rather small. The resistance looks nearly constant. This is due to the integration of the transmission when calculating conductance. Notably, a very similar result would occur if the transmission coefficient were identical everywhere, including

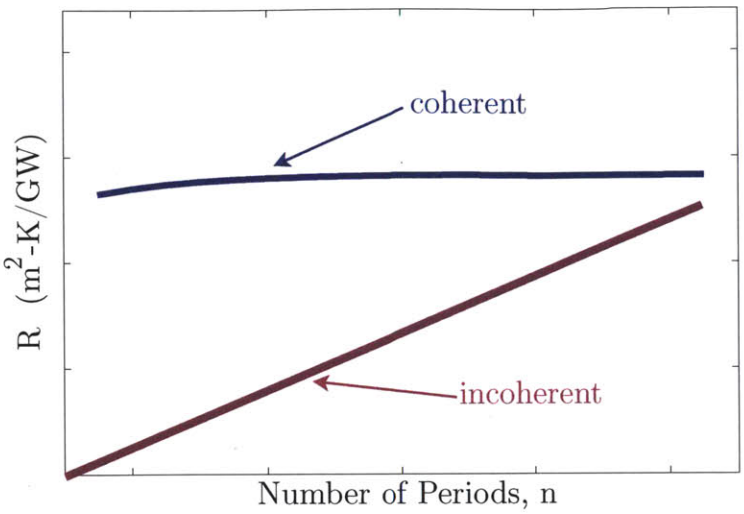

Figure 2-10: Trends for thermal resistance in the cases that cross-plane thermal transport is diffusive or coherent. If thermal transport is fully coherent, the resistance trend is dominated by the transmissivity of phonons through the SL. Since GaAs and AlAs are well lattice-matched, the phonon transmissivity increases very slightly as the period number is increased. Thus, the resistance is approximately constant, with a very slight change in the first several periods when the stopbands form. When thermal transport is fully diffusive, an equivalent thermal resistor is added for each additional period, so total thermal resistance grows monotonically with increasing period number.

if the transmission coefficient were uniformly unitary. This situation would arise if there were no acoustic impedance mismatch, since it is this mismatch that was used in the TMM to calculate the reflection and transmission probability of a phonon. If the ratio of acoustic impedances of the materials on either side of the interface is one, then according to Eq. 2.9, the reflection coefficient is zero, so the transmission coefficient is one. This is the situation where instead of a SL, there is simply a slab of uniform material.

2.1.5 Lattice Thermal Conductivity

The effective lattice thermal conductivity is determined from the thermal conductance, as calculated above, and the geometry of the sample. The thermal conductance of the sample, as determined from the Landauer-Büttiker formalism, is the reciprocal

of the more commonly used thermal resistance,

$$K = 1/R. \tag{2.13}$$

The thermal resistance, then, is related to the thermal conductivity of a material or a nanostructure through the geometry of the sample. The thermal resistance determined from the above calculations is shown in Fig. 2-10. The thermal conductivity of the SL based on coherent transport, k_{eff}, is related to the thermal resistance by

$$k_{eff} = L/RA. \tag{2.14}$$

The thickness of the sample depends on the number of layers, n, and the thickness of the superlattice period, d_1. Thus, the conductance is related to the thermal conductivity of the sample through

$$K = k_{eff}A/n * d_1. \tag{2.15}$$

Finally, by combining the Landauer-Büttiker formalism and the more general definition of thermal conductance as given above, the thermal conductivity of the sample is found to be

$$k_{eff} = nd_1 \sum_p \int_0^\omega \tau_{\omega,eff} v_p C_{ave}\, d\omega. \tag{2.16}$$

The thermal conductivity of the nanostructure is, thus, linearly proportional to the thickness of the sample, and the integrated frequency-dependent transmissivity of phonons through the sample, and is shown in Fig. 2-11.

GaAs and AlAs were chosen as the material system for this experiment based on their good lattice matching. This property makes them easy to grow epitaxially using molecular organic chemical vapor deposition (MOCVD). This good lattice matching is also the reason that the stop-bands, as seen in Fig. 2-8, are so thin. Due to the relatively small contribution of the stop-bands, the integrated transmissivity through the SL changes relatively little as the stop-bands form with increasing number of

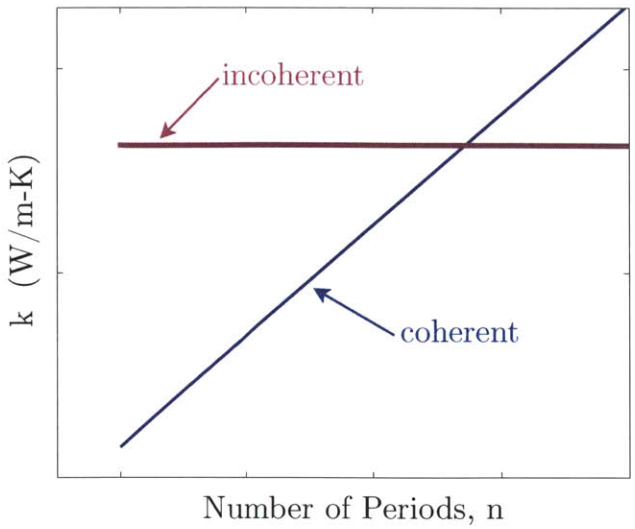

Figure 2-11: Trends for thermal conductivity in the cases that cross-plane thermal transport is fully diffusive or fully coherent.

periods. This relatively small change in the phonon transmissivity corresponds to a similarly minor change in conductance as determined by the Landauer-Büttiker formalism. Since the thermal conductivity is proportional to the nearly constant thermal conductance, and is also proportional to the thickness of the SL, it is the linearly increasing thickness of the SL that dominates the thermal conductivity trend. Thus, when coherent phonon transport is dominant, the thermal conductivity grows linearly with increasing period number.

2.2 Thermal Properties due to Diffusive Transport

The Landauer-Büttiker formalism, which treats energy transport as a transmission process, can be applied in both the coherent and incoherent regime. In both cases, it is necessary to determine a transmission coefficient. In the coherent regime, wave mechanics can be used, as was done in the previous section. In the diffusive regime, all phase information is lost and scattering at an interface is diffuse. The loss of phase information excludes the use of wave mechanics to determine the transmission coefficient. Finding the transmission, then, becomes very complicated and it is no

longer advantageous to use the Landauer-Büttiker formalism.

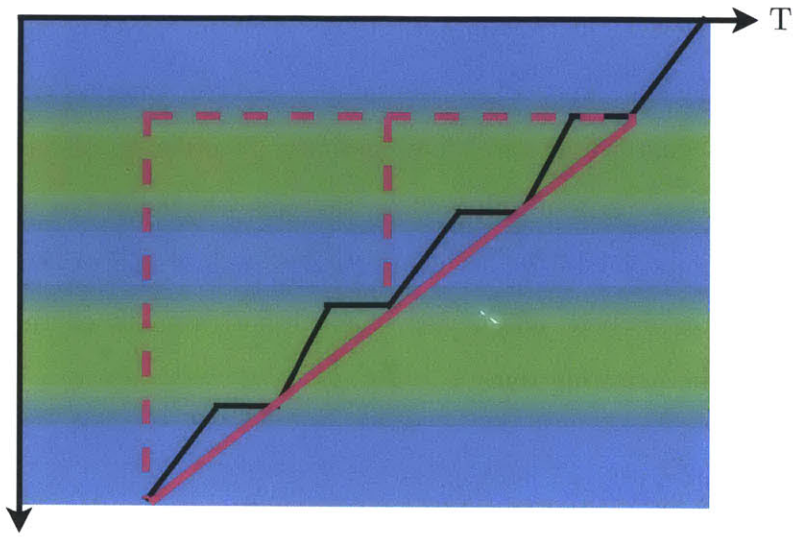

Figure 2-12: In the diffusive picture of transport, a local thermal equilibrium is assumed everywhere. This suggests that within the layers, there is a linear temperature drop whose gradient depends on the thermal transport properties of the individual layers. At the interface, there is a temperature drop due to the Kapitza resistance. Thus, the overall temperature profile within the superlattice is staggered, as shown in the figure. However, if each AlAs layer, GaAs layer, and interface is assumed to be identical, a coarse-grained picture shows a linear temperature drop whose slope does not change with changing number of periods. This constant slope corresponds to a constant thermal conductivity.

Instead, in the fully diffusive transport regime, local thermal equilibrium is assumed everywhere, corresponding to a linear temperature drop through each material, as well as a temperature drop at the interface. Though these temperature drops are discontinuous, since the periods are identical and repeating and the interfaces are all the same, it is possible to coarse-grain the picture, revealing a linear temperature drop through the SL nanostructure (Fig. 2-12). The slope of this temperature drop, corresponding to the thermal conductivity of the sample, does not change with increasing numbers of periods. Thus, the thermal conductivity in the case of fully diffusive transport, is constant (Fig. 2-11). The thermal resistance, which depends on the monotonically increasing thickness of the sample and the constant thermal conductivity of the sample, thus also grows monotonically with increasing SL period number, again in contrast to the approximately constant thermal resistance in the

fully coherent case.

In conclusion, if coherent transport is the dominant thermal transport mechanism, the thermal conductivity will rise monotonically with the number of periods in the SL. If, however, diffusive transport is dominant, then the thermal conductivity will be constant with an increasing number of periods. In order to test this hypothesis, the thermal conductivity of five different SL samples was measured using an optical pump-and-probe technique. In the following chapter, this transient thermoreflectance experiment will be explained, along with the method used to extract the thermal conductivity from the resulting data.

Chapter 3

Experimental Investigation

A time-domain thermoreflectance (TDTR) experiment is used to measure the thermal transport properties of the superlattices (SLs) under investigation. In the TDTR, or pump-and-probe, setup, a laser pulse called the 'pump' pulse impinges upon a material, exciting electrons at the surface. Within hundreds of femtoseconds, these electrons thermalize, thereby increasing the lattice temperature through electron-phonon collisions [72, 73]. The excited phonons then propagate through the sample, carrying heat away from the surface, thus decreasing the sample surface temperature. The change in temperature in a material is related to its change in reflectivity via the thermoreflectance coefficient. Thus, as the surface temperature changes, so will the surface reflectivity. This reflectivity is measured by another, much weaker, laser pulse called the 'probe' pulse. By changing its optical path length with a mechanical delay stage, the probe pulse can be delayed in time relative to the pump pulse to measure the transient surface reflectivity and, thus, the temperature. The curve traced out by the surface temperature through time can then be fit to the analytical solution of the heat equation at the surface of the sample, based on its thermal properties. In this chapter, the experimental system will be described, along with the analysis used to extract thermal properties based on the results of the experiment.

3.1 Pump-and-Probe Experimental System

The first pump-and-probe experiment to measure thermal diffusivity was performed by Paddock and Eesley at the General Motors Research Lab in 1986. They used a pump laser pulse with a wavelength of 633 nm and a full-width half-maximum (FWHM) of 8 ps, and a probe laser pulse of wavelength 595 nm and a FWHM of 6 ps, giving them ps-scale time resolution [74]. In 1996, Capinski and Maris worked on solving problems of beam divergence and alignment difficulty by implementing an optical fiber in their pump-and-probe experiment. The single-mode optical fiber removed noise in the beam associated with the movement of the mechanical delay stage. Additionally, by only using one laser and splitting the output of that laser, they further decreased the noise and increased their time-resolution because the single dye laser produced a sub-ps pulse [75]. Cahill *et al.* employed a titanium-doped sapphire (Ti:Sapph) laser to produce 150 fs pulses, giving them the highest temporal resolution achieved to date. To simplify the use of the pump-and-probe, they added a CCD camera to visualize the sample. They made several additions to improve the signal-to-noise ratio of their signal. The pump-and-probe experiment devised by Cahill *et al.* is still considered state of the art, and is replicated closely in this thesis project [76].

The pump-and-probe experimental system is located in the Rohsenow Kendall Heat Transfer Laboratory and was constructed by a previous Ph.D. student, Dr. Aaron Schmidt. A more detailed explanation of both the system and the subsequent signal analysis can be found in his thesis [77]. A schematic diagram of the TDTR experimental system is shown in Fig. 3-1. The output of an 80 MHz Ti:Sapph laser, 200 fs pulses centered around a wavelength of 800 nm, passes through an optical isolator to prevent potentially destabilizing reflections back into the laser. The time-averaged output power of the Ti:Sapph laser is approximately 1.5 W. After passing through the isolator, the laser beam carries about 1.4 W. The laser beam then passes through a polarizer followed by a half-wave plate (HWP). Together, these two optical elements act as an adjustable beam-splitter, allowing for a tunable amount of the

laser power to be directed into the pump arm, while the remaining power goes into the probe arm. Past the HWP, the two arms follow different paths.

About 1.2 W is split off and becomes the pump beam, which goes through an electro-optic modulator (EOM) that modulates the beam to enable lock-in detection. After the pump beam passes through the EOM, it passes through a beta Barium Borate (BBO) frequency-doubling crystal which, through non-linear optical effects, converts the 800 nm input light to 400 nm output light with an efficiency of about 20%. The pump then passes through an adjustable telescope, allowing it to have a variable focused spot size. Finally, the pump passes through a 10x telescope objective lens before impinging on the sample. This lens focuses the pump light onto the sample.

After being split off from the initial laser source, the probe beam follows a path regulated by a mechanical delay stage. The delay stage changes the probe beam's optical path length, thus controlling the difference in time between when the pump pulse, with a constant path length, and the probe pulse, with a variable path length, arrive at the sample. Our setup is able to create a time-delay of about 7 ns. After the delay stage, the probe arm also passes through the microscope objective to focus it onto the sample surface. After hitting the sample, some of the pump and some of the probe light will reflect off of the sample.

It is important to isolate the reflected probe light from the much stronger pump light, because the information we are interested in analyzing is embedded in the weaker probe light. The pump light needs to be completely filtered so that it does not overwhelm the reflected probe signal. Since they are different colors, optical elements with selective coatings are used to filter the reflected probe light from the reflected pump light. The filtered probe light then impinges upon an amplified Si photodetector and generates an electric potential, the magnitude of which depends upon the intensity of the reflected light. Using lock-in detection, the change caused by the pump, which occurs at the EOM modulation frequency, is isolated from the large DC background reflectivity of the sample.

The pump-and-probe experiment is performed both at room temperature and at low temperatures, yielding temperature-dependent information about the thermal

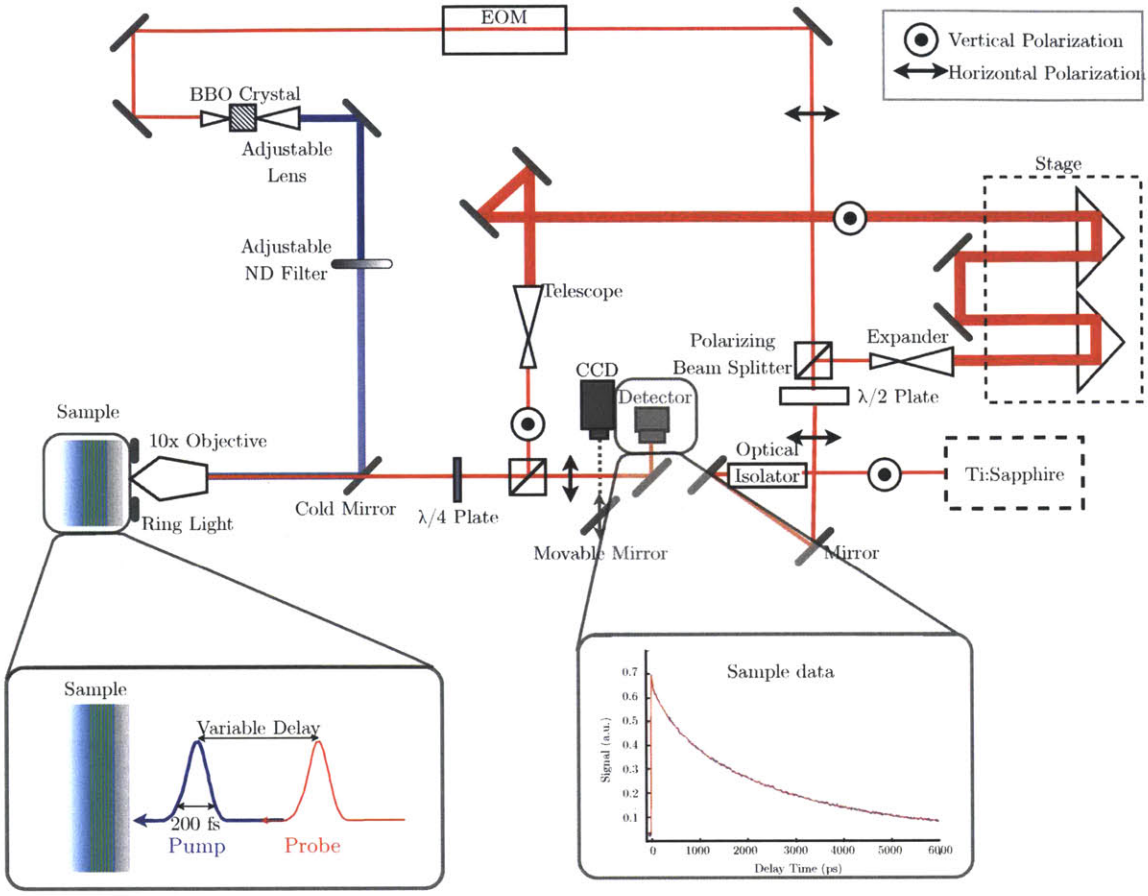

Figure 3-1: Diagram of the pump-and-probe experimental system used for this study.

transport properties of the samples being measured. The sample is placed inside of a cryostat attached to a turbopump vacuum capable of achieving vacuum pressure on the order of 10^{-5} Torr. Coolant such as liquid He or N_2 flows through the cold finger embedded in the cryostat. A temperature controller measuring the temperature inside of the cold finger actively regulates the current passing through a resistive heater attached to the cold finger. The temperature is measured with a Si diode mounted to the surface of the sample. Temperatures as low as 8 K can be achieved with this system.

3.2 Data Analysis

To determine the thermal transport parameters of interest, we use a multi-dimensional least-squares minimization routine to match a model of the predicted temperature decay based on Fourier's law to the data gathered using the pump-and-probe setup. The mathematical model used is an application of linear time-invariant system theory which we use to extract the thermal transfer function of the sample, $Z(\omega)$. This thermal transfer function relates the modulated heat input, $H(\omega)$, to the resulting temperature of the surface of the sample. The following section outlines how the thermal response is found by solving the Fourier heat equation in cylindrical coordinates. Then the transfer function will be described, followed by the relationship between this thermal transfer function and the output of the lock-in amplifier.

3.2.1 Thermal Model

The sample is modeled as a multi-layer stack with a periodic heat flux at the surface. Such a multi-layer solution can be constructed by combining the solutions for each constituent layer. A thorough derivation of the solution to this heat transfer problem can be found in *Conduction of Heat in Solids* by Carslaw and Jaeger [78]. Solving the heat equation for a single layer of thickness d and thermal diffusivity α (Fig. 3-2) yields a matrix equation for the temperature, Θ_n, and heat flux, f_n, on the bottom of the layer as a function of the temperature, Θ_{n-1}, and heat flux, f_{n-1}, on the top of the layer where the heating is taking place,

$$\begin{bmatrix} \Theta_n \\ f_n \end{bmatrix} = \begin{bmatrix} cosh(qd) & -\frac{1}{\kappa_z q} sinh(qd) \\ -\kappa_z q sinh(qd) & cosh(qd) \end{bmatrix} \begin{bmatrix} \Theta_{n-1} \\ f_{n-1} \end{bmatrix} \tag{3.1}$$

where κ_z is the through-plane thermal conductivity, and $\alpha = \kappa_z/\rho C$ is the through-plane thermal diffusivity such that $q = \sqrt{i\omega/\alpha}$. This matrix equation comes from the solution to the heat equation for steady, periodic heating, omitting the time factor, $e^{i\omega t}$, where ω is the heating modulation frequency.

In the limit where the heat capacity of a layer is zero, this matrix solution applies

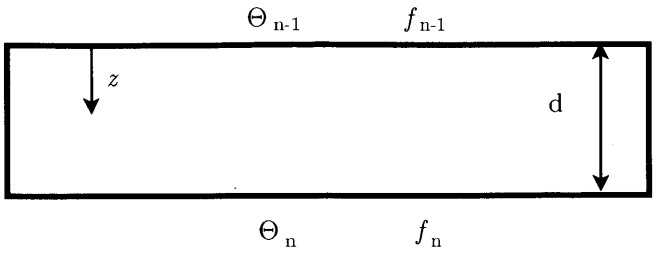

Figure 3-2: Heat equation boundary conditions for a single layer. Θ is the temperature on a particular side, f is the heat flux, and d is the thickness of the layer.

for heat flowing across an interface, whose conductance is finite due to the complicated interactions between phonons on either side of a boundary between dissimilar materials [28]. Each interface, then, counts as a separate layer with a conductance, G. The matrix equation for heat transfer through an interface is similar to eq. (3.1) except the heat capacity, C, is zero. This matrix is given by

$$\begin{bmatrix} \Theta_n \\ f_n \end{bmatrix} = \begin{bmatrix} 1 & G^{-1} \\ 0 & 1 \end{bmatrix} \begin{bmatrix} \Theta_{n-1} \\ f_{n-1} \end{bmatrix}. \tag{3.2}$$

It is immediately clear that $G = \kappa_z/d$ and the heat flux on either side of the interface is equal, i.e. $f_n = f_{n-1}$. G is called the thermal interface conductance (TIC).

For heat flow through n such layers (Fig. 3-3), the product of the matrices for each layer yields an equation for the temperature, Θ_n, and heat flux, f_n, at the end of the stack as a function of the temperature, Θ_0, and heat flux, f_0, at the surface of the stack,

$$\begin{bmatrix} \Theta_n \\ f_n \end{bmatrix} = \mathbf{M_n M_{n-1} M_{n-2} ... M_1} = \begin{bmatrix} A & B \\ C & D \end{bmatrix} \begin{bmatrix} \Theta_0 \\ f_0 \end{bmatrix}. \tag{3.3}$$

The reflected probe signal is analogous to the temperature of the surface of the

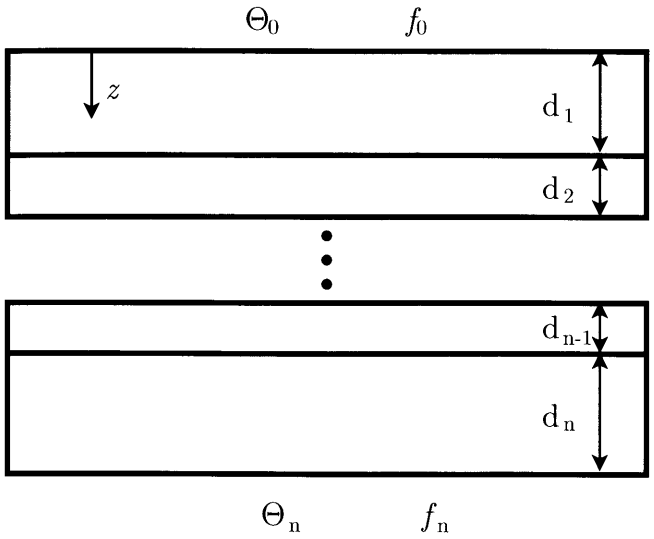

Figure 3-3: Heat equation boundary conditions for a multi-layer stack. The conditions are known at the top of the stack and at the bottom of the stack and can be determined for the rest of the layers by solving a matrix version of the heat equation.

sample, or Θ_0. Thus, we would like to solve for this quantity as a function of the physical parameters of the sample. To simplify the analysis, the back of the sample is assumed to be adiabatic; in other words, the sample is assumed to be infinitely thick in our configuration. This assumption can be checked simply by determining the thermal penetration depth and how it compares to the thickness of the sample. For steady, periodic heating, the thermal penetration depth can be estimated by $L = \sqrt{\alpha/2\omega_0}$ where ω_0 is the frequency of the periodic heating. In our TDTR setup, this frequency varies between roughly 1 MHz and 10 MHz, and α is typically in the range of $1e{-}6$ m^2/s. This yields a penetration depth on the order of hundreds of nm. This penetration depth, much smaller than the laser spot size of roughly 60 μm, also allows us to treat transport as one-dimensional [79, 80]. The samples used in this study were grown on GaAs wafers that are 300 μm thick, thus the last layer more than satisfies the condition for an adiabatic boundary. Because the last layer is considered to be adiabatic, or $f_n = 0$, the above matrix equation can be simplified to

$$C\Theta_0 + Df_0 = 0. \tag{3.4}$$

where f_0 is the known periodic heat flux applied to the surface of the stack. Thus, only the constants D and C, dependent on the thermal properties of the layers, are necessary to solve for the surface temperature, Θ_0, of the sample.

This analysis can also be performed using the heat equation in cylindrical coordinates. We shall briefly explain this analysis since it more closely matches the geometry of the TDTR experiment, where the pump spot has cylindrical symmetry [81]. The heat equation in cylindrical coordinates in the frequency domain is

$$\frac{\partial^2\theta(\omega)}{\partial z^2} = q_0^2\theta(\omega) \tag{3.5}$$

and is identical to the one dimensional heat equation in the frequency domain. The only difference between the solution to the heat equation through a multilayer stack in cylindrical coordinates is a modified q, q_0

$$q_0^2 = \frac{\kappa_r k^2 + \rho c i\omega}{\kappa_z} \tag{3.6}$$

where κ_r is the thermal conductivity in the radial direction. In this solution, k is the Hankel transform variable, used to simplify the analysis of the radial heat conduction equation. This q_0 is then applied to equations (3.1) - (3.4) to find the surface temperature of the sample with cylindrical symmetry in heating,

$$\Theta_0 = -\frac{D}{C} f_0. \tag{3.7}$$

The periodic heating at the surface, f_0, is given by

$$f_0 = \frac{A_0}{2\pi} \exp\left(\frac{-k^2\omega_0^2}{8}\right) \tag{3.8}$$

Thus, the surface temperature in the Hankel transform domain is given by

$$\Theta_0(k) = -\frac{D}{C}\frac{A_0}{2\pi} \exp\left(\frac{-k^2\omega_0^2}{8}\right) \tag{3.9}$$

Finally, by including the spatial distribution of the heating, a single integral that can be solved numerically is obtained for the thermal response of the system, $H(\omega)$,

the frequency dependent temperature of the surface of the sample

$$H(\omega) = \frac{A_0}{2\pi} \int_0^\infty k\left(-\frac{D}{C}\right) \exp\left(\frac{-k^2(w_0^2 + w_1^2)}{8}\right) dk \tag{3.10}$$

where A_0 is the absorbed probe power, and w_0 and w_1 are the $1/e^2$ radii of the pump and the probe beams, respectively. This is the thermal response of the system to periodic heating at the surface and represents the integrated radial temperature distribution of the surface layer.

3.2.2 Extracting Thermal Properties from TDTR Data

The probe signal can be described by a transfer function, $Z(\omega_0)$, whose amplitude and phase depend upon the thermal response of the system as well as the characteristics of the probe arm. The transfer function $Z(\omega_0)$ relates the input signal, a periodic heating of frequency ω_0, to the amplitude, R, and phase, ϕ, of the response:

$$Re^{i(\omega_0 t + \phi)} = Z(\omega_0)e^{i\omega_0 t}. \tag{3.11}$$

This equation clearly shows the relationships between the phase and the amplitude of the signal and the transfer function are

$$R = |Z(\omega_0)| \tag{3.12}$$

and

$$\phi = arg(Z(\omega_0)). \tag{3.13}$$

Both the magnitude and the phase of the response will depend upon the delay between the pump pulse and the probe pulse. The result of measuring the response of the sample with a delayed probe pulse is to give us an instant view of the state of the thermal system at the specific delay time. By gathering information on the state of the system with a high time resolution between 0 ns and 6 ns of delay, we add redundancy to the measurements. Rather than simply having the two points

in time necessary to solve the transient heat equation, we gather a large collection of such points and can thus find a best fit to the entire cooling curve. The lock-in receives the signal of the unmodulated probe pulse. By mixing this signal with a sinusoid at the modulation frequency, the lock-in can reject all other frequency components. Our lock-in amplifier rejects all frequency components outside of a 10 Hz band around the reference frequency [82]. The probe frequency is the same as the laser frequency, 80 MHz, well outside of the chosen modulation frequency ω_0, which is usually between 3 and 12 MHz. By mixing the input to the detector with a cosine wave at the modulation frequency, the lock-in is able to extract the in-phase, X, component of the signal; mixing with a sine wave yields the out-of-phase, or Y, component of the signal. The in-phase and out-of-phase components determine the amplitude and phase of the response of the sample, where the amplitude is given by

$$R^2 = X^2 + Y^2 \tag{3.14}$$

and the phase by

$$\phi = tan^{-1}\left(\frac{Y}{X}\right). \tag{3.15}$$

The transfer function itself can be determined from linear-time invariant (LTI) theory and depends upon the thermal impulse response of the system, $H(\omega)$ as prescribed by eg. (3.10). The transfer function is

$$Z(\omega_0) = \frac{\beta Q Q_{probe}}{T^2} \sum_{k=-\infty}^{\infty} H(\omega_0 + k\omega_s) e^{ik\omega_s \tau} \tag{3.16}$$

where β is the thermoreflectance coefficient, Q is the energy per pump pulse, Q_{probe} is the energy per probe pulse, T is the time between pump pulses, ω_0 is the modulation frequency, ω_s is the probe sampling frequency, in our case the frequency of the laser output, 80 MHz, and τ is the delay-time between the pump and the probe pulses. Again, by gathering an entire data collection with a variety of different time delays between 0 and 6 ns, we are able to achieve a more robust fitting to the data. Although the properties of the top layer of material and the laser have an effect on the absolute

magnitude of the signal and thus on the signal to noise ratio (SNR), in the data analysis, the lock-in signal is normalized such that the properties: β, Q, Q_{probe}, T, and A, on which the thermal transport properties of interest should not depend, fall out of the transfer function.

We have derived the model of the signal detected by the lock-in that depends only upon the thermal transport properties of the sample and the modulation frequency of the heating. A multi-dimensional least-squares algorithm is used to find the thermal transport properties of the sample by matching this model to the experimentally retrieved data.

3.3 Superlattice Fabrication

The SLs used in this experiment were fabricated by a student in the Fitzgerald Group in the Materials Science and Engineering Department at MIT using molecular-organic chemical vapor deposition (MOCVD). AlAs and GaAs were chosen as the constituents of the SL because they are relatively simple to grow using this technique. The samples were prepared in accordance with what the theory described in Ch. 2 suggested would give the best results from the TDTR experiments. Thus, five samples of one period, three periods (Fig. 3-4), five periods, seven periods, and nine periods of GaAs/Alas SL were grown. Additionally, a sample of the wafer on which the SLs were grown was provided by the Fitzgerald Group.

Initially, a GaAs buffer layed is deposited on a GaAs wafer with a 6° offcut at a temperature of 650 °C under an Arsine over pressure, which prevents the decomposition of the surface due to Arsine's volatility. The superlattice, consisting of alternating layers of 12 nm of GaAs and 12 nm of AlAs, is grown at a temperature of 750 °C. These thicknesses were chosen based on a sensitivity analysis of the TTR experiment. The sensitivity results indicated that a balance had to be met between the thickness of the total SLs and the individual thicknesses of the layers. The layers should, ideally, be kept to a minimum thickness to prevent any potential bulk scattering within the materials. However, the overall SL thickness needed to be maximized so that the

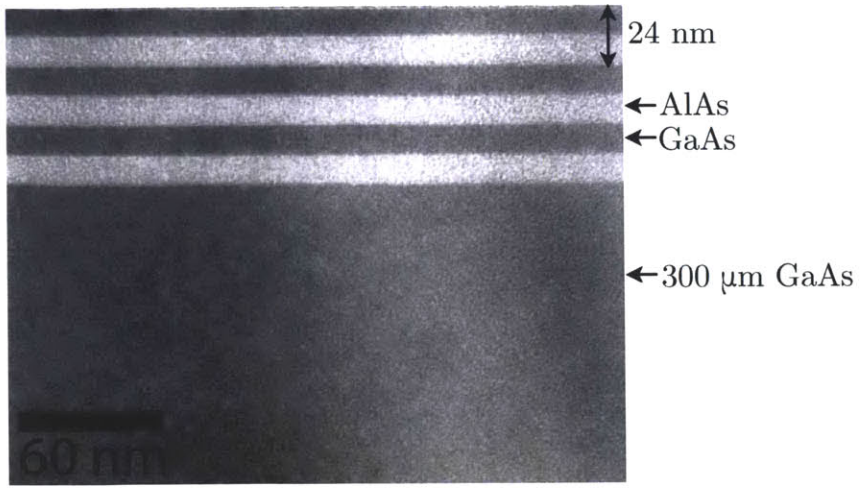

Figure 3-4: This is a cross-sectional TEM image of one of the periodic structures used for this study. This particular sample is 3 period of 12 nm GaAs/12 nm AlAs on a 300 μm GaAs wafer.

signal would be sensitive to the SL rather than the surrounding thermal resistances. The sensitivity analysis yielded a layer thickness of 12 nm as a reasonable compromise between these two opposing requirements. As the temperature is ramped up, the GaAs buffer layed continues to be deposited, reaching a total of thickness of about 500 nm. Once the temperature has stabilized, the SL is grown [83].

Approximately 100 nm of Al was deposited on the surface of the samples using e-beam evaporation at the Microsystems Technology Lab (MTL) at MIT. The metal layer acts as a thermal-optical transducer material because of its high thermoreflectance coefficient and small absorption depth. A very small change in temperature produces a high change in reflectivity at our probe wavelength of 800 nm [84]. A short absorption depth on the order of 10 nm ensures that no photon absorption is happening in the sample. Finally, a high Schottke barrier between Al and GaAs greatly decreases the chances that any excited electrons pass from the Al layer to the semiconductor layer, so no electron effects need to be considered during the heating of the sample.

The thickness is chosen based on previous studies that have shown the highest

accuracy in TDTR results when the metal film was between 80 and 130 nm thick. [56]. The thickness of the deposited Al layer was measured both with a Dektak profilometer, and using a calibration technique. In the calibration, a sample of sapphire is coated with Al at the same time as the samples to be measured. TDTR is then used to determine the thermal conductivity of the sapphire. The thickness of the Al layer parameter is adjusted until the measured sapphire thermal conductivity matches the known literature value. Both of these thickness measurement techniques yielded a value of 98 nm of Al, with small variations around this number.

Chapter 4

Results and Discussion

Time domain thermoreflectance measurements were made to determine the thermal transport properties of five GaAs/AlAs SL samples. In order to observe coherent wave effects with this measurement technique, each sample had a different number of periods—1, 3, 5, 7, and 9—with each period consisting of 12 nm of GaAs and 12 nm of AlAs grown with MOCVD. The samples were measured at a range of temperatures between 30 K and 296 K, with cryogenic temperatures achieved with liquid He and liquid N_2 cooling under vacuum conditions. Five locations were measured per sample with four pump modulation frequencies for each location. A multi-dimensional least squares minimization routine was used to fit the average of five measurements to a multilayer Fourier law heat transfer model to determine the unknown properties of interest as presented in Chapter 3. A sample data set is shown in Fig. 4-1. The results of the measurements and the data fitting are presented in this chapter.

4.1 Data Fitting

The data were fit to a Fourier model of heat transport through a four layer stack. The four layers are the aluminum optical transducer layer, the interface between the Al and the SL, the SL, and the GaAs substrate, where the GaAs substrate, at 300 μm thick, is modeled as a semi-infinite layer. Defects, strain, and roughness at the interface between the SL and the substrate are minimal compared to the Al-SL

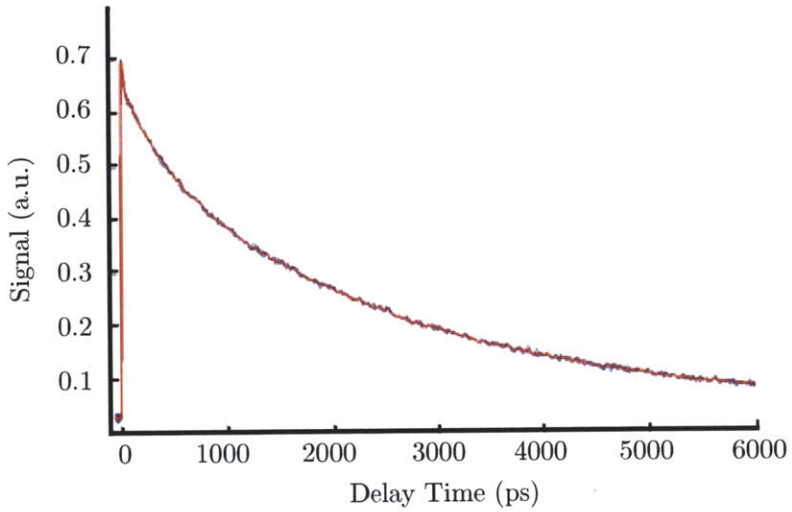

Figure 4-1: This is the data generated by measuring the thermoreflectance signal of a five period SL at 50K at a modulation frequency of 3 MHz. The blue lines are individual measurements and the red line is the resulting average of these three measurements.

interface due to the SL's and the substrate's good lattice matching and the epitaxial nature of the growth process, and the corresponding resistance of this interface is thus neglected.

As outlined in Chapter 3, the solution to the thermal model depends on the thickness of each layer, its heat capacity, its thermal conductivity, and the anisotropy of the thermal conductivities in the in-plane direction versus the through-plane direction. The heat capacity of the SL is the weighted average of the heat capacities of AlAs and GaAs [56]. The temperature-dependent literature values for heat capacity and thermal conductivity are shown in Appendix A in Fig. A-1 and A-2. Recent studies on nanoscale heat transport through semiconductor materials have shown that the thermal conductivities of these materials are smaller than bulk values previously reported in the literature [85]. To determine whether this effect was also present in GaAs, TTR measurements of the thermal conductivity of a GaAs wafer were conducted. The results are shown in Fig. 4-2. The results clearly show that at low temperatures there is a decrease in the thermal conductivity of the GaAs wafer compared to literature values under the conditions of the TTR experiment. Thus, in

the fittings for the thermal conductivity of the SL, the measured values of GaAs from these experiments were used rather than the values found in literature.

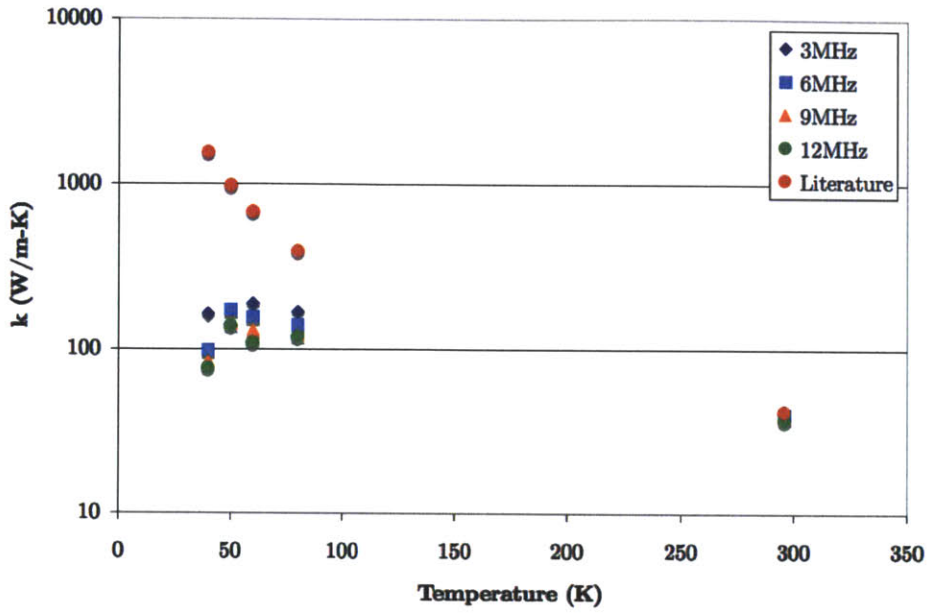

Figure 4-2: A comparison of literature and measured values for the thermal conductivity of GaAs. Recent experiments have shown that the conditions of the TTR experiment lead to a deviation from accepted values of thermal conductivity due to ballistic transport [85]. The results of this measurement were included in the fitting parameters of the experimental SL data.

4.2 Results

Five locations were measured on each sample at four different modulation frequencies. For this experimental setup, the modulation frequencies that have shown the highest accuracy and the lowest signal to noise ratios are in the range between 3 MHz and 12 MHz [77]. Thus, the thermal transport properties of the SLs were measured at each location at modulation frequencies of 3 MHz, 6 MHz, 9 MHz, and 12 MHz. Each measurement consisted of the average of five runs. No systematic frequency-dependent trend was visible in the data, as indicated by Fig. 4-3. As a result, the rest of the data presented herein represents the averaging of data from both different

locations and at different modulation frequencies. In other words, each data point represents the average of 60 pump-and-probe measurements.

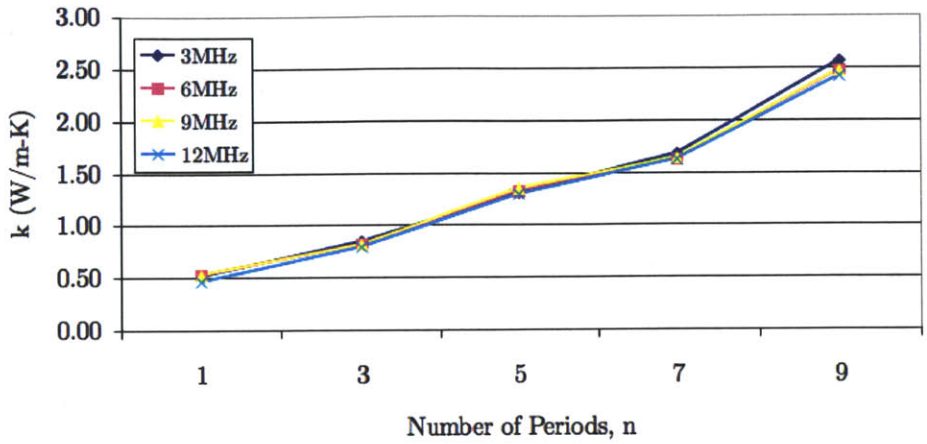

Figure 4-3: Measured thermal conductivity of SLs at 30K as a function of the number of periods and at each modulation frequency. No systemic frequency dependence was observed at this or any other temperature.

The temperature dependent thermal conductivities of the five samples are shown in Fig. 4-4 and the values for the temperature-dependent thermal interface conductances (TIC) are shown in Fig. 4-5. The temperature-dependent thermal conductivity shows a consistent trend in all of the samples, a large increase in thermal conductivity with temperature between 30K and 100K, followed by a leveling out. The change in thermal conductivity with temperature increases as the number of periods in the SL increases. At 30K, the ratio of the thermal conductivity of the nine period sample to the thermal conductivity of the one-period sample is about five. At 100K, this ratio is 12. Between 200K and 300K, the thermal conductivities of the one, three, five, and seven period SLs all grow by approximately the same amount.

Between 150K and 300K, the seven and nine-period samples clearly exhibit the same behavior—dipping to a lower thermal conductivity, and then increasing again. A similar dip is actually present in all of the samples, though the amplitude of the decrease as well as the temperature at which it occurs is different. The five period sample appears to have a small dip at 200K, the three period at 150 K, and the one period at 100K. However, the size of the dips in these cases is small enough to be

within the margin of error of the measurement and the fitting, and thus may just be an artifact of the technique.

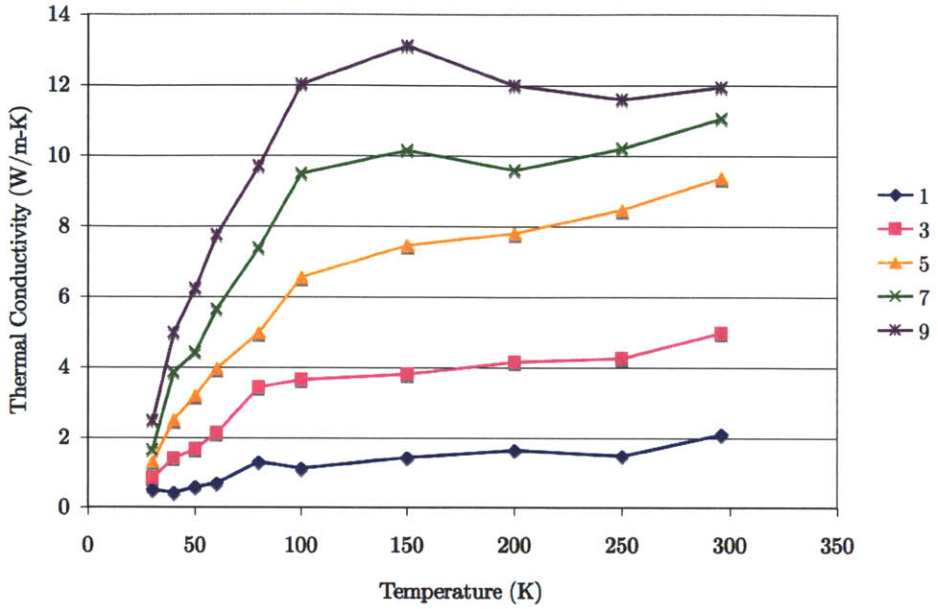

Figure 4-4: Measure thermal conductivity of SLs with different numbers of periods as a function of temperature.

The temperature-dependent TIC between the Al optical transducer layer and the SL sample are shown in Fig. 4-5. Since all of the samples were grown under similar conditions, and Al was deposited on them simultaneously, it is expected that the TICs of all the samples should be equal at every temperature. However, this is far from what the data indicate. In fact, the data shows a wide variation in the TICs of every sample. Even when TIC data from the most widely varying sample, the one-period SL, is removed, as in Fig. 4-6, there is still large variation among the samples.

The reason for the large variation in the TIC is the relative insensitivity of the fitting to the TIC. This insensitivity can be demonstrated by varying the parameters in the fitting and looking at the variation in the resulting cooling curve, as is done in Fig. 4-7. In this figure, the open red circles are the thermoreflectance signal of a five period SL measured at a pump modulation frequency of 3 MHz and a temperature of 50 K. The blue curves in both figures represent the best-fit curves yielded by the multi-dimensional, least-squares fitting program, and correspond to the thermal

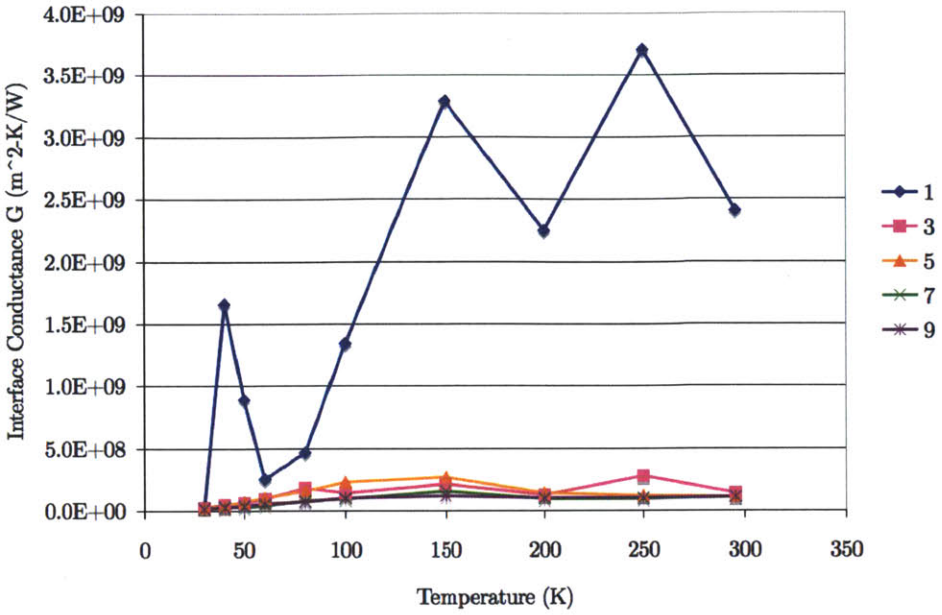

Figure 4-5: Measured thermal interface conductance (TIC) between the Al optical transducer layer and the SL for SLs of varying period numbers. Although it is expected that the TIC should not be a function of number of SL periods, as this graph indicates, the fitting did not show a strong sensitivity to the interface conductance. Thus, these values may be simply artifacts of the fitting program.

conductivities and TICs shown in Figs. 4-4, 4-5, 4-6, and 4-8. In (a), the solid red line and green line correspond to the curves that would result from a decrease and increase, respectively, by 10% of the SL thermal conductivity. In (b), the solid red and green lines correspond to a decrease and increase, respectively, by 10% of the Al-SL TIC. The difference between these three curves is much greater in (a) than in (b), showing that the fitting is more sensitive to the SL thermal conductivity than the TIC. Although the resulting curves are different for each SL and at each temperature, this general trend was observed for all cases. Thus, although the TIC data are disparate, this analysis shows that this may just be an artifact of the fitting rather than an indication that there may be something wrong with the data. Further examples of this measurement insensitivity are given in Appendix A.

The dependence of the thermal conductivity of the SLs with respect to the number of periods in the SLs at every temperature value measured is given in Fig. 4-8. This graph clearly shows an overall increasing trend in the thermal conductivity

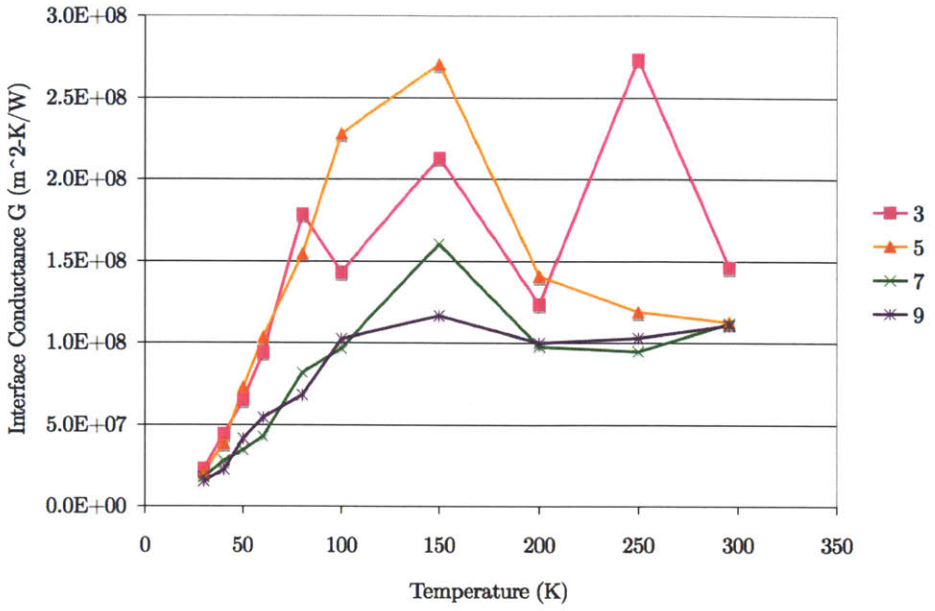

Figure 4-6: Measured TIC between the Al optical transducer layer and the SL for three, five, seven, and nine period SLs.

with number of layers. At lower temperatures, this increase is linear, as expected if coherent transport were dominant, while at temperatures of 200K, 250K, and 296K, there is clearly some non-linearity, as would be expected for diffusive transport.

This data set is a strong indication of the presence of coherent phonon wave effects in SLs, a phenomenon that has not been previously observed in experiments.

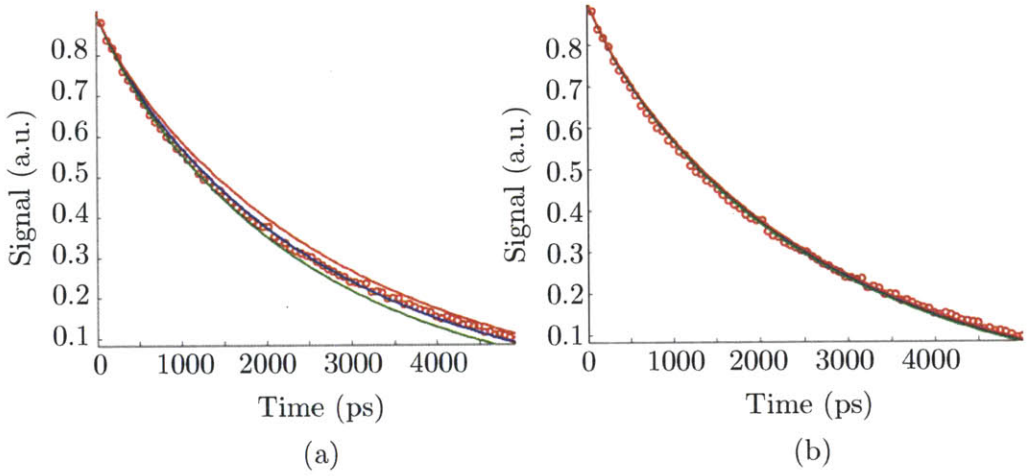

Figure 4-7: Data and fitting curves for five period SL at 50K and at a modulation frequency of 3 MHz. The open red circles are data points, in (a) the blue solid line is the curve corresponding to the parameters yielded by the fitting analysis, the red curve represents the curve corresponding to a 10% smaller thermal conductivity while the green curve represents the curve corresponding to a 10% greater thermal conductivity; in (b) the three curves—red, green, and blue—represent different TICs and all lie on top of one another, demonstrating the relative insensitivity of the fitting with respect to the TIC.

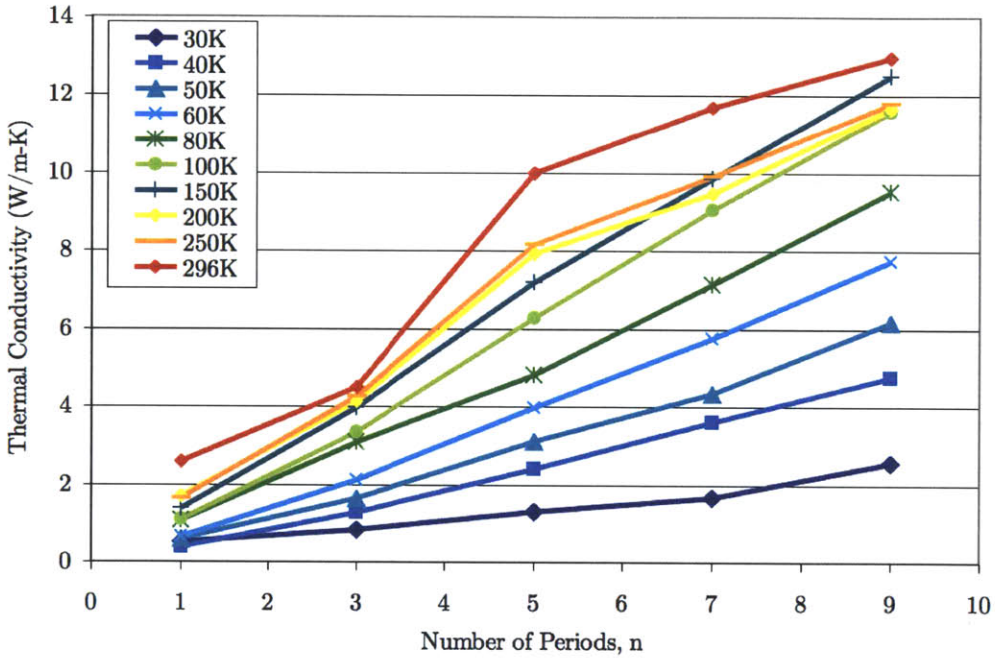

Figure 4-8: Measured thermal conductivity of SLs as a function of number of periods at different temperatures.

Chapter 5

Summary and Future Work

5.1 Summary

A detailed experiment to detect coherent wave effects in superlattices using an optical pump-and-probe technique is described. Superlattices are invaluable learning tools for a great deal of applications, from optoelectronics to power generation, and give great insight into the fundamental processes behind thermal transport. This thesis adds to the existing volume of knowledge about SLs by probing the possible existence of coherent wave effects, never before seen experimentally.

The Landauer-Büttiker formalism, which treats transport as a transmission process, is used to quantitatively determine the expected trend in thermal conductivity in a GaAs/AlAs SL if coherent effects are present. The results show that, due to the close acoustic impedances of the constituent materials, the conductance of the SL does not change very much with increasing numbers of periods. The conductivity, which is given by the product of the thickness of the SL and its conductance, grows proportionally to the thickness, which increases linearly with the number of periods. This linear growth in the thickness dominates the expected thermal conductivity trend. Thus, if coherent effects are present, the thermal conductivity is expected to increase linearly with number of periods.

The thermal conductivities of five SL samples with period numbers ranging from one to nine are measured with a transient thermoreflectance (TTR) experiment. The

results of the experiment are matched to the predicted cooling behavior of a multilayer stack given by Fourier's conduction law. A multi-dimensional least-squares fit to the thermal model yields the thermal conductivity of the SL sample.

The results show the presence of coherent wave effects at lower temperatures, and a decrease in the presence of coherent wave effects at higher temperatures. These results represent the first experimental confirmation of the presence of coherent wave effects in thermal transport.

5.2 Future Work

This experiment and the resulting findings are unique in the body of work relating to SL thermal conductivity. Previous experiments varied the size of the layers but held the thickness of the SL constant, and the thickness of the overall structure was much greater than the thermal penetration depths of the experiments used to measure them. In this experiment, the thicknesses of the SL period was held at a constant 24 nm, comprised of 12 nm of GaAs and 12 nm of AlAs, but the number of periods was varied from one to nine. The thermal conductivity was measured for these samples at temperature ranging from 30K to 296K. The results of the experiment showed, for the first time, the presence of coherent wave effects in SLs. This exciting result leads to a number of potential future directions.

According to the calculations performed in Chapter 2, the linear growth in thermal conductivity should occur whether or not a SL is present, if the transmission-based picture presented by the Landauer-Büttiker formalism accurately describes the transport through the SL. As was noted before, the integrated phonon transmissivity change very little with the addition of periods. As a result, the conductance for each of the five SLs measured is nearly the same, and the linear trend in the data is due almost completely to the growth in the thickness of the SL. To determine conductivity, the calculated conductance is multiplied by this thickness. If the conductance is constant and the thickness grows linearly, the conductivity will also grow linearly until the thickness of the material or structure is greater than phonon MFPs. This is

the effect of boundary scattering. Although this is a different effect than the buildup of the dispersion relation, it is nevertheless due to coherent transport through the SL. Thus, coherent effects are seen in the experiment, although it is impossible to distinguish which effect it is.

This discrepancy can be clarified experimentally by measuring the thermal conductivity of progressively thicker thin films instead of SLs. If boundary scattering is dominant, a linear trend in the thermal conductivity of the thin films should be as noticeable as the thermal conductivity trend in the SLs. If wave interference effects are the dominant driving force behind the linear trend seen in the SL results, they should be absent in the thin film, where no wave interference should occur.

In addition, many assumptions were made in order to simplify the calculations of the thermal conductivity trend. To achieve a more accurate and quantitative prediction, these simplification must be lifted. The original assumptions were that all phonons were normally incident onto the SL interfaces and thus there was no phonon mode conversion, the interfaces were perfect specular scatterers, only one direction was taken in calculating both the phonon group velocities, and the heat capacities, and these values were averaged for GaAs and AlAs. These simplifications enabled a relatively simple implementation of the Landauer-Büttiker formalism for determining the thermal conductivity of the SLs. Although the calculation revealed a very specific trend, the values for the conductivities were very far off as a result of the assumptions.

More quantitative analysis and experimental tests are needed to better understand the results of this experiment. However, the presence of coherent wave effects has been detected for the first time with this experiment. These results add another important layer to the growing knowledge of thermal transport properties at the nanoscale.

Appendix A

Data fittings

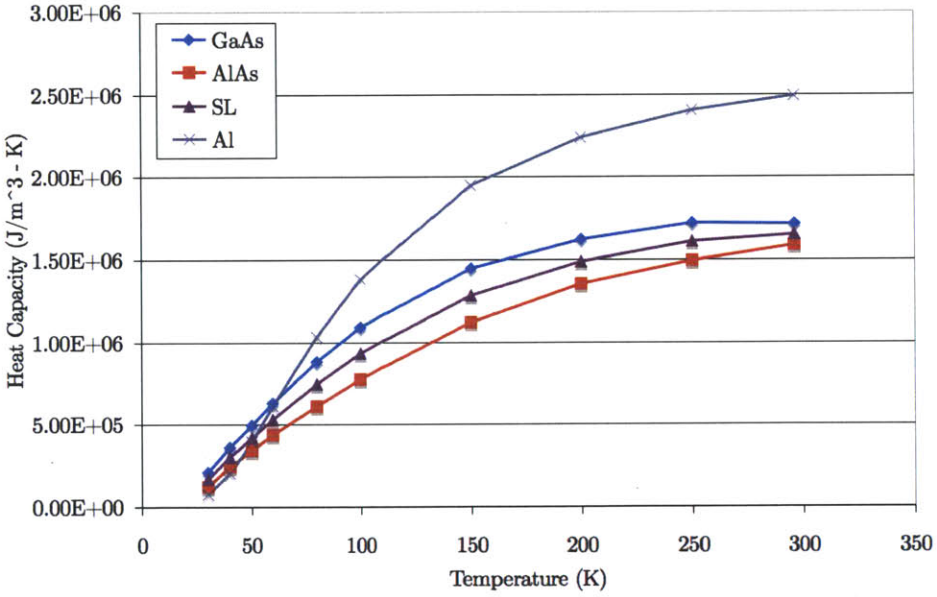

Figure A-1: Literature values for temperature dependent heat capacities of Al, GaAs, and AlAs. The SL heat capacity us assumed to be the average of GaAs and AlAs.

The following are sample data fittings used to determine the thermal conductivities of the five SL samples. The open red circles show the data. The blue line is the line of best fit. The red and green lines represent what the fitting would look like if a certain property deviated from its fitted value by 10%.

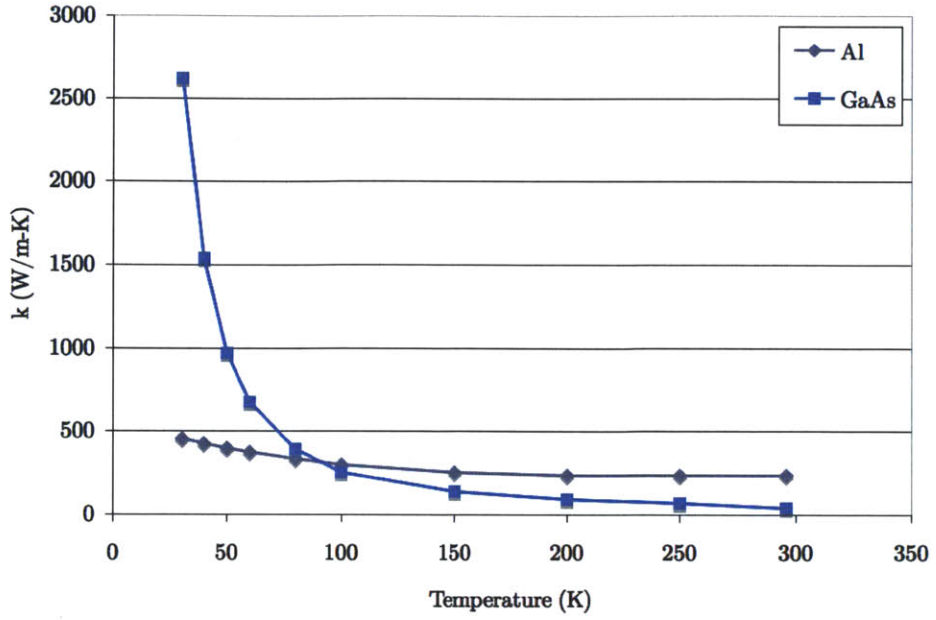

Figure A-2: Literature values for temperature dependent thermal conductivity of Al, and GaAs.

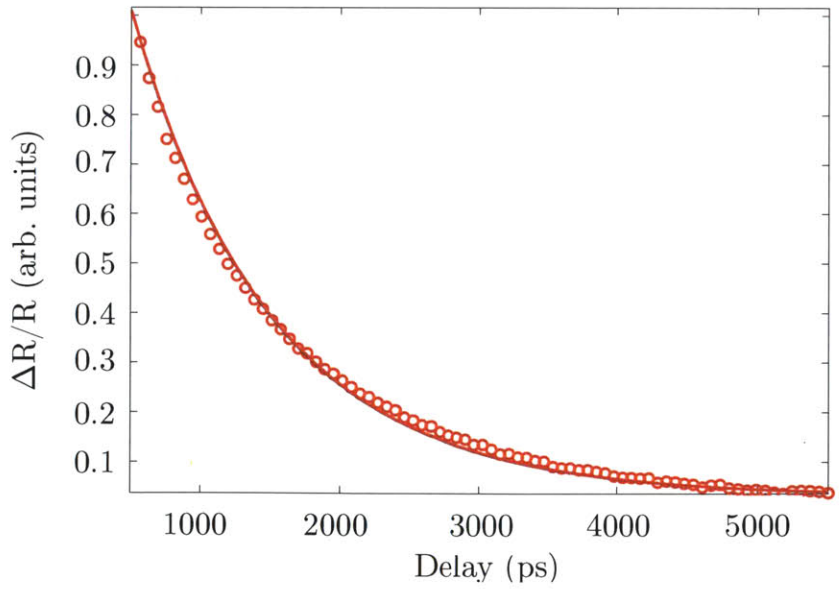

Figure A-3: Data fitting to a 1 pd. SL at 30K with red and green lines showing the result of varying the Al-SL thermal interface conductance. The lines are not visible because this dataset is insensitive to the thermal interface conductance. All three of the lines (blue, red, and green) all lie on top of one another.

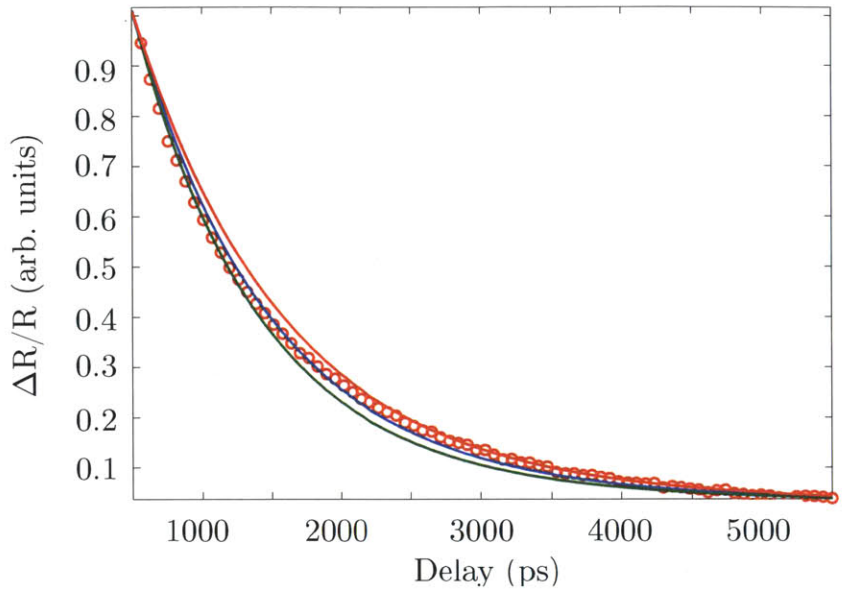

Figure A-4: Data fitting to a 1 pd. SL at 30K with red and green lines showing the result of varying the SL thermal conductance. Unlike Fig. A-3, the lines representing a deviation from the fitted thermal conductivity are visible. This indicates that the measurement is, in fact, sensitive to the SL thermal conductivity.

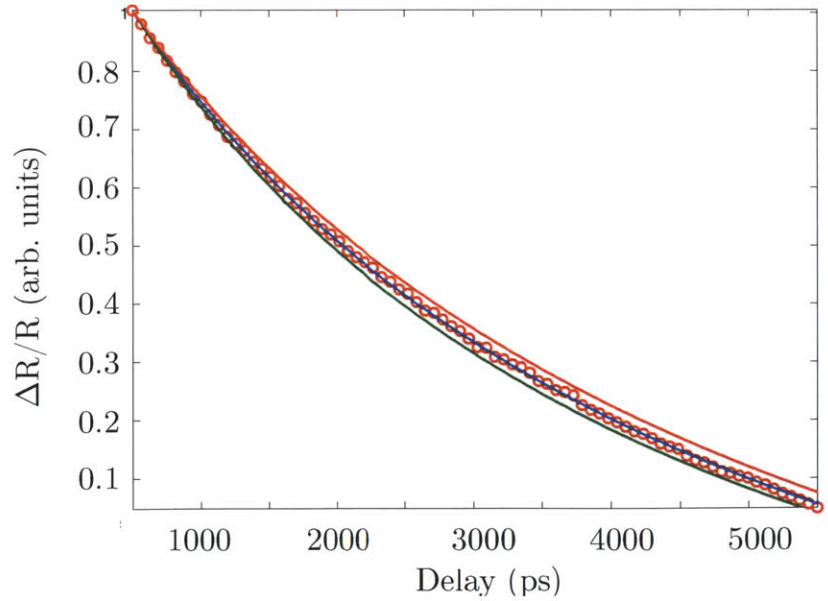

Figure A-5: Data fitting to a 1 pd. SL at 296K with red and green lines showing the result of varying the Al-SL thermal interface conductance.

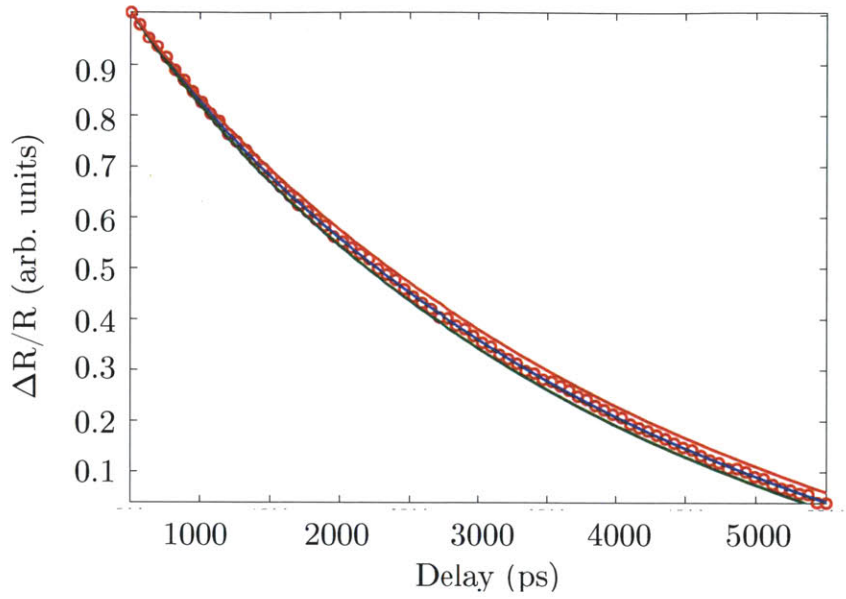

Figure A-6: Data fitting to a 1 pd. SL at 296K with red and green lines showing the result of varying the SL thermal conductivity.

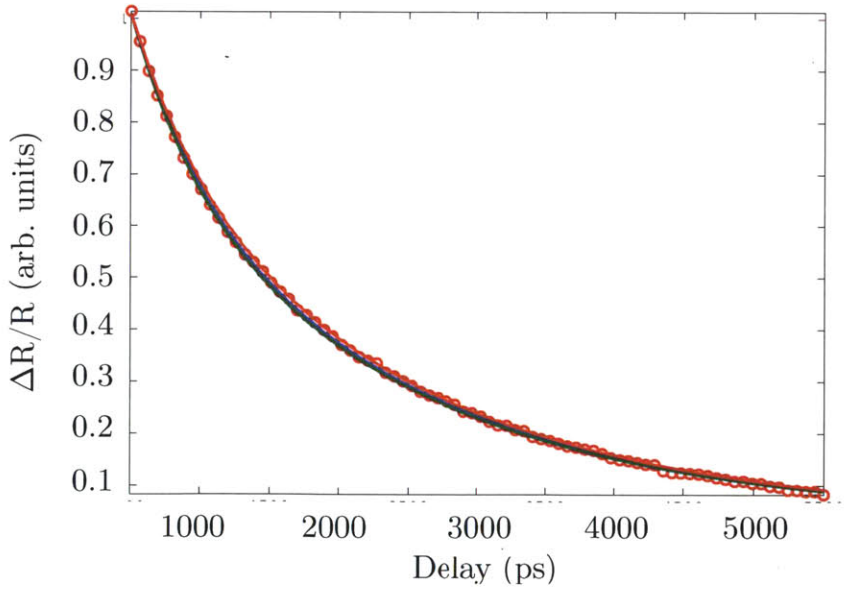

Figure A-7: Data fitting to a 9 pd. SL at 30K with red and green lines showing the result of varying the Al-SL thermal interface conductance by 10%. This dataset is largely insensitive to the thermal interface conductance, with all three of the lines (blue, red, and green) all lying very nearly on top of one another.

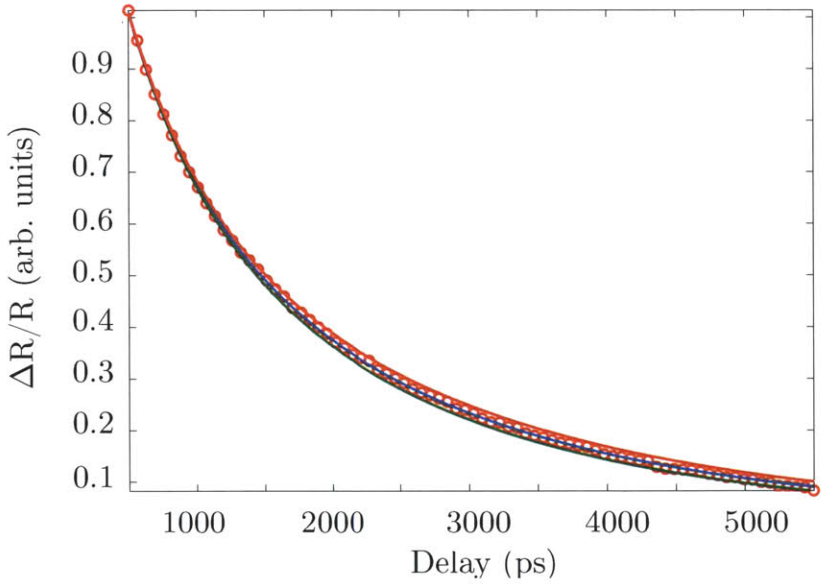

Figure A-8: Data fitting to a 9 pd. SL at 30K with red and green lines showing the result of varying the SL thermal conductivity by 10%.

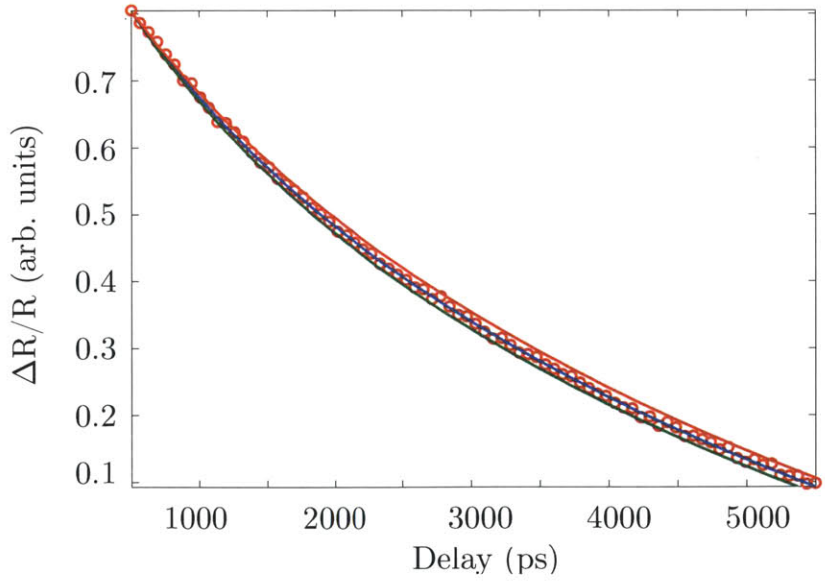

Figure A-9: Data fitting to a 9 pd. SL at 296K with red and green lines showing the result of varying the Al-SL thermal interface conductance by 10%.

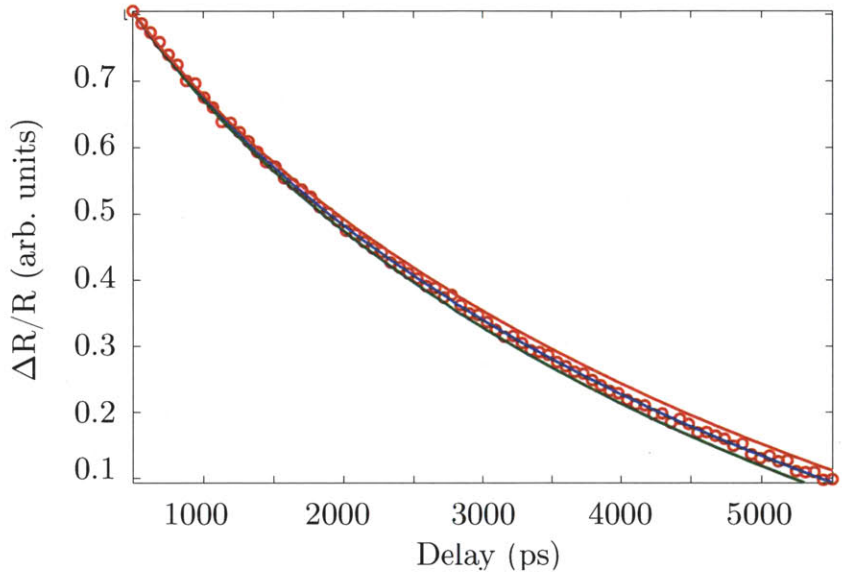

Figure A-10: Data fitting to a 9 pd. SL at 296K with red and green lines showing the result of varying the SL thermal conductivity by 10%.

Bibliography

[1] R. Schaller, "Moore's law: past, present and future," *Spectrum, IEEE*, vol. 34, pp. 52 –59, Jun. 1997.

[2] H. J. Caulfield and S. Dolev, "Why future supercomputing requires optics," *Nature Photonics*, vol. 4, pp. 261–263, May 2010.

[3] L. Esaki and R. Tsu, "Superlattice and negative differential conductivity in semiconductors," *IBM Journal of Research and Development*, vol. 14, pp. 61 –65, Jan. 1970.

[4] I. K. Schuller, "New class of layered materials," *Phys. Rev. Lett.*, vol. 44, pp. 1597–1600, Jun. 1980.

[5] Q. S. Yang, C. M. Falco, and I. K. Schuller, "Tunneling studies of a metallic superlattice," *Phys. Rev. B*, vol. 27, pp. 3867–3870, Mar. 1983.

[6] R. P. Andres, J. D. Bielefeld, J. I. Henderson, D. B. Janes, V. R. Kolagunta, C. P. Kubiak, W. J. Mahoney, and R. G. Osifchin, "Self-assembly of a two-dimensional superlattice of molecularly linked metal clusters," *Science*, vol. 273, no. 5282, pp. 1690–1693, 1996.

[7] K. Ploog and G. H. Dohler, "Compositional and doping superlattices in III-V semiconductors," *Advances in Physics*, vol. 32, no. 3, pp. 285–359, 1983.

[8] G. Chen, C. Tien, C. Wu, and J. Smith, "Thermal diffusivity measurements of GaAs/AlGaAs thin-film structures," *J. Heat Transfer*, vol. 116, pp. 325–331, May 1994.

[9] E. Wiener-Avnear, "Artificially engineered pyroelectric $Sr_{1-x}Ba_xTiO_3$ superstructure films," *Applied Physics Letters*, vol. 65, pp. 1784 –1786, Oct. 1994.

[10] C. H. Raymond Ooi, T. C. Au Yeung, C. H. Kam, and T. K. Lim, "Photonic band gap in a superconductor-dielectric superlattice," *Phys. Rev. B*, vol. 61, pp. 5920–5923, Mar. 2000.

[11] M. N. Touzelbaev, P. Zhou, R. Venkatasubramanian, and K. E. Goodson, "Thermal characterization of Bi_2Te_3/Sb_2Te_3 superlattices," *Journal of Applied Physics*, vol. 90, no. 2, pp. 763–767, 2001.

[12] I. Chowdhury, R. Prasher, K. Lofgreen, G. Chrysler, S. Narasimhan, R. Mahajan, D. Koester, R. Alley, and R. Venkatasubramanian, "On-chip cooling by superlattice-based thin-film thermoelectrics," *Nature Nanotechnology*, vol. 4, pp. 235–238, 2009.

[13] R. Venkatasubramanian, E. Siivola, T. Colpitts, and B. O'Quinn, "Thin-film thermoelectric devices with high room-temperature figures of merit," *Nature*, vol. 413, pp. 597–602, 2001.

[14] C. Collier, T. Vossmeyer, and J. Heath, "Nanocrystal superlattices," *Annu. Rev. Phys. Chem.*, vol. 49, pp. 371–404, 1998.

[15] B. Liang, X. Guo, J. Tu, D. Zhang, and J. Cheng, "An acoustic rectifier," *Nature Materials*, vol. 9, pp. 989–992, 2010.

[16] B. Liang, B. Yuan, and J.-c. Cheng, "Acoustic diode: Rectification of acoustic energy flux in one-dimensional systems," *Phys. Rev. Lett.*, vol. 103, p. 104301, Sep. 2009.

[17] T. Soga, S. Hattori, S. Sakai, M. Takeyasu, and M. Umeno, "MOCVD growth of GaAs on Si substrates with AlGaP and strained superlattice layers," *Electronics Letters*, vol. 20, pp. 916 –918, Oct. 1984.

[18] R. Venkatasubramanian, T. Colpitts, B. O'Quinn, S. Liu, N. El-Masry, and M. Lamvik, "Low-temperature organometallic epitaxy and its application to superlattice structures in thermoelectrics," *Applied Physics Letters*, vol. 75, no. 8, pp. 1104–1106, 1999.

[19] J. Faist, F. Capasso, D. L. Sivco, C. Sirtori, A. L. Hutchinson, and A. Y. Cho, "Quantum cascade laser," *Science*, vol. 264, no. 5158, pp. 553–556, 1994.

[20] B. Saleh and M. Teich, *Fundamentals of Photonics*. Wiley, 2007.

[21] L. D. Hicks and M. S. Dresselhaus, "Effect of quantum-well structures on the thermoelectric figure of merit," *Phys. Rev. B*, vol. 47, pp. 12727–12731, May 1993.

[22] L. D. Hicks, T. C. Harman, and M. S. Dresselhaus, "Use of quantum-well superlattices to obtain a high figure of merit from nonconventional thermoelectric materials," *Applied Physics Letters*, vol. 63, no. 23, pp. 3230–3232, 1993.

[23] J. O. Sofo and G. D. Mahan, "Thermoelectric figure of merit of superlattices," *Applied Physics Letters*, vol. 65, no. 21, pp. 2690–2692, 1994.

[24] G. Bastian, A. Vogelsang, and C. Schiffmann, "Isotopic superlattices for perfect phonon reflection," *Journal of Electronic Materials*, vol. 39, pp. 1769–1771, 2010. 10.1007/s11664-010-1160-1.

[25] R. Venkatasubramanian, "Lattice thermal conductivity reduction and phonon localizationlike behavior in superlattice structures," *Phys. Rev. B*, vol. 61, pp. 3091–3097, Jan. 2000.

[26] X. Fan, G. Zeng, C. LaBounty, J. E. Bowers, E. Croke, C. C. Ahn, S. Huxtable, A. Majumdar, and A. Shakouri, "SiGeC/Si superlattice microcoolers," *Applied Physics Letters*, vol. 78, no. 11, pp. 1580–1582, 2001.

[27] M. Lundstrom, *Fundamentals of Carrier Transport.* Cambridge University Press, 2000.

[28] D. G. Cahill, W. K. Ford, K. E. Goodson, G. D. Mahan, A. Majumdar, H. J. Maris, R. Merlin, and S. R. Phillpot, "Nanoscale thermal transport," *Journal of Applied Physics*, vol. 93, no. 2, pp. 793–818, 2003.

[29] A. J. Minnich, *Exploring electron and phonon transport at the nanoscale for thermoelectric energy conversion.* PhD thesis, Massachusctts Institute of Technology, 2011.

[30] J. Garg. Personal communication, Jan. 2012.

[31] S.-M. Lee and D. G. Cahill, "Heat transport in thin dielectric films," *Journal of Applied Physics*, vol. 81, no. 6, pp. 2590–2595, 1997.

[32] E. Conwell and V. F. Weisskopf, "Theory of impurity scattering in semiconductors," *Phys. Rev.*, vol. 77, pp. 388–390, Feb. 1950.

[33] P. Nath and K. Chopra, "Thermal conductivity of copper films," *Thin Solid Films*, vol. 20, no. 1, pp. 53 – 62, 1974.

[34] T. Ruf, J. Spitzer, V. F. Sapega, V. I. Belitsky, M. Cardona, and K. Ploog, "Interface roughness and homogeneous linewidths in quantum wells and superlattices studied by resonant acoustic-phonon raman scattering," *Phys. Rev. B*, vol. 50, pp. 1792–1806, Jul. 1994.

[35] P. L. Kapitza, "Heat transfer and superfluidity of helium II," *Phys. Rev.*, vol. 60, pp. 354–355, Aug. 1941.

[36] G. L. Pollack, "Kapitza resistance," *Rev. Mod. Phys.*, vol. 41, pp. 48–81, Jan. 1969.

[37] P. M. Norris and P. E. Hopkins, "Examining interfacial diffuse phonon scattering through transient thermoreflectance measurements of thermal boundary conductance," *Journal of Heat Transfer*, vol. 131, no. 4, p. 043207, 2009.

[38] A. Baerker, M. J.L., and G. A.C., "Study of zone-folding effects on phonons in alternating monolayers of GaAs-AlAs," *Phys. Rev. B*, vol. 17, pp. 3181–3196, Apr. 1978.

[39] V. Narayanamurti, H. L. Störmer, M. A. Chin, A. C. Gossard, and W. Wiegmann, "Selective transmission of high-frequency phonons by a superlattice: The "dielectric" phonon filter," *Phys. Rev. Lett.*, vol. 43, pp. 2012–2016, Dec. 1979.

[40] S.-k. Yip and Y.-C. Chang, "Theory of phonon dispersion relations in semiconductor superlattices," *Phys. Rev. B*, vol. 30, pp. 7037–7059, Dec. 1984.

[41] S.-i. Tamura, Y. Tanaka, and H. J. Maris, "Phonon group velocity and thermal conduction in superlattices," *Phys. Rev. B*, vol. 60, pp. 2627–2630, Jul. 1999.

[42] P. Hyldgaard and G. D. Mahan, "Phonon superlattice transport," *Phys. Rev. B*, vol. 56, pp. 10754–10757, Nov. 1997.

[43] W. E. Bies, R. J. Radtke, and H. Ehrenreich, "Phonon dispersion effects and the thermal conductivity reduction in GaAs/AlAs superlattices," *Journal of Applied Physics*, vol. 88, no. 3, pp. 1498–1503, 2000.

[44] D. A. Broido and T. L. Reinecke, "Lattice thermal conductivity of superlattice structures," *Phys. Rev. B*, vol. 70, p. 081310, Aug. 2004.

[45] S. Y. Ren and J. D. Dow, "Thermal conductivity of superlattices," *Phys. Rev. B*, vol. 25, pp. 3750–3755, Mar. 1982.

[46] G. Srivastava, *The Physics of Phonons*. Taylor & Francis Group, 1990.

[47] M. V. Simkin and G. D. Mahan, "Minimum thermal conductivity of superlattices," *Phys. Rev. Lett.*, vol. 84, pp. 927–930, Jan 2000.

[48] B. Yang and G. Chen, "Partially coherent phonon heat conduction in superlattices," *Phys. Rev. B*, vol. 67, p. 195311, May 2003.

[49] G. Chen and M. Neagu, "Thermal conductivity and heat transfer in superlattices," *Applied Physics Letters*, vol. 71, no. 19, pp. 2761–2763, 1997.

[50] G. Chen, "Thermal conductivity and ballistic-phonon transport in the cross-plane direction of superlattices," *Phys. Rev. B*, vol. 57, pp. 14958–14973, Jun. 1998.

[51] S. Volz, J. Saulnier, G. Chen, and P. Beauchamp, "Computation of thermal conductivity of Si/Ge superlattices by molecular dynamics techniques," *Microelectronics Journal*, vol. 31, no. 9-10, pp. 815 – 819, 2000.

[52] A. Chomette, B. Deveaud, A. Regreny, and G. Bastard, "Observation of carrier localization in intentionally disordered GaAs/GaAlAs superlattices," *Phys. Rev. Lett.*, vol. 57, pp. 1464 –1467, Sep. 1986.

[53] T. Yao, "Thermal properties of AlAs/GaAs superlattices," *Applied Physics Letters*, vol. 51, pp. 1798 –1800, Nov. 1987.

[54] W. Capinski and H. Maris, "Thermal conductivity of GaAs/AlAs superlattices," *Physica B: Condensed Matter*, vol. 219-220, pp. 699 – 701, 1996. PHONONS 95, Proceedings of the Combined Conference of the 4th International Conference on Phonon Physics and the 8th International Conference on Phonon Scattering in Condensed Matter.

[55] S.-M. Lee, D. G. Cahill, and R. Venkatasubramanian, "Thermal conductivity of Si-Ge superlattices," *Applied Physics Letters*, vol. 70, pp. 2957 –2959, Jun. 1997.

[56] W. S. Capinski, H. J. Maris, T. Ruf, M. Cardona, K. Ploog, and D. S. Katzer, "Thermal-conductivity measurements of GaAs/AlAs superlattices using a picosecond optical pump-and-probe technique," *Phys. Rev. B*, vol. 59, pp. 8105–8113, Mar. 1999.

[57] X. Y. Yu, G. Chen, A. Verma, and J. S. Smith, "Temperature dependence of thermophysical properties of GaAs/AlAs periodic structure," *Applied Physics Letters*, vol. 67, no. 24, pp. 3554–3556, 1995.

[58] S. T. Huxtable, A. R. Abramson, C.-L. Tien, A. Majumdar, C. LaBounty, X. Fan, G. Zeng, J. E. Bowers, A. Shakouri, and E. T. Croke, "Thermal conductivity of Si/SiGe and SiGe/SiGe superlattices," *Applied Physics Letters*, vol. 80, no. 10, pp. 1737–1739, 2002.

[59] Y. Imry and R. Landauer, "Conductance viewed as transmission," *Rev. Mod. Phys.*, vol. 71, pp. S306–S312, Mar. 1999.

[60] Y. Gao, A. Marconnet, M. Panzer, S. LeBlanc, S. Dogbe, Y. Ezzahri, A. Shakouri, and K. Goodson, "Nanostructured interfaces for thermoelectrics," *Journal of Electronic Materials*, vol. 39, pp. 1456–1462, 2010. 10.1007/s11664-010-1256-7.

[61] G. Chen, *Nanoscale Energy Transport and Conversion.* Oxford, 2005.

[62] S. Tamura and J. P. Wolfe, "Acoustic-phonon transmission in quasiperiodic superlattices," *Phys. Rev. B*, vol. 36, pp. 3491–3494, Aug. 1987.

[63] G. Chen, "Phonon wave heat conduction in thin films and superlattices," *Journal of Heat Transfer*, vol. 121, no. 4, pp. 945–953, 1999.

[64] V. B. Antonyuk, M. Larsson, A. G. Mal'shukov, and K. A. Chao, "Phonon transmission in iiiv semiconductor superlattices and alloys," *Semiconductor Science and Technology*, vol. 20, no. 5, p. 347, 2005.

[65] D. G. Sedrakyan and A. G. Sedrakyan, "Localization of phonons in a two-component superlattice with random-thickness layers," *Phys. Rev. B*, vol. 60, pp. 10114–10121, Oct. 1999.

[66] S. Mizuno and S.-i. Tamura, "Theory of acoustic-phonon transmission in finite-size superlattice systems," *Phys. Rev. B*, vol. 45, pp. 734–741, Jan. 1992.

[67] D. A. Broido, M. Malorny, G. Birner, N. Mingo, and D. A. Stewart, "Intrinsic lattice thermal conductivity of semiconductors from first principles," *Applied Physics Letters*, vol. 91, no. 23, p. 231922, 2007.

[68] J. S. Blakemore, "Semiconducting and other major properties of gallium arsenide," *Journal of Applied Physics*, vol. 53, no. 10, pp. R123–R181, 1982.

[69] D. Wright and R. Cobbold, "Acoustic wave transmission in time-varying phononic crystals," *Smart Materials and Structures*, vol. 18, no. 1, p. 015008, 2009.

[70] H. Kato, H. J. Maris, and S.-i. Tamura, "Resonant-mode conversion and transmission of phonons in superlattices," *Phys. Rev. B*, vol. 53, pp. 7884–7889, Mar. 1996.

[71] S. Adachi, *GaAs and Related Materials: Bulk Semiconducting and Superlattice Properties.* World Scientific Publishing Company, Inc., 1995.

[72] T. Qiu and C. Tien, "Short-pulse laser heating on metals," *International Journal of Heat and Mass Transfer*, vol. 35, no. 3, pp. 719 – 726, 1992.

[73] T. Q. Qiu and C. L. Tien, "Heat transfer mechanisms during short-pulse laser heating of metals," *Journal of Heat Transfer*, vol. 115, no. 4, pp. 835–841, 1993.

[74] C. A. Paddock and G. L. Eesley, "Transient thermoreflectance from metal films," *Optics Letters*, vol. 11, no. 5, p. 273, 1986.

[75] W. S. Capinski and H. J. Maris, "Improved apparatus for picosecond pump-and-probe optical measurements," *Rev. Sci. Instrum*, vol. 67, no. 8, p. 2720, 1986.

[76] D. G. Cahill, K. Goodson, and A. Majumdar, "Thermometry and thermal transport in micro/nanoscale solid-state devices and structures," *Journal of Heat Transfer*, vol. 124, no. 2, pp. 223–241, 2002.

[77] A. J. Schmidt, *Optical characterization of thermal transport from the nanoscale to the macroscale.* PhD thesis, Massachusetts Institute of Technology, 2008.

[78] H. Carslaw and J. Jaeger, *Conduction of Heat in Solids*, pp. 64–70, 109–112. Oxford University Press, 1959.

[79] P. E. Hopkins, J. R. Serrano, L. M. Phinney, S. P. Kearney, T. W. Grasser, and C. T. Harris, "Criteria for cross-plane dominated thermal transport in multilayer thin film systems during modulated laser heating," *Journal of Heat Transfer*, vol. 132, no. 8, p. 081302, 2010.

[80] A. J. Schmidt, X. Chen, and G. Chen, "Pulse accumulation, radial heat conduction, and anisotropic thermal conductivity in pump-probe transient thermoreflectance," *Review of Scientific Instruments*, vol. 79, pp. 114902 –114902–9, Nov. 2008.

[81] D. G. Cahill, "Analysis of heat flow in layered structures for time-domain thermoreflectance," *Review of Scientific Instruments*, vol. 75, pp. 5119 –5122, Dec. 2004.

[82] Stanford Research Systems, "User's manual: Model SR844 RF lock-in amplifier," 2003.

[83] A. Jandl. Personal communication, Dec. 2011.

[84] M. Burzo, P. Komarov, and P. Raad, "Minimizing the uncertainties associated with the measurement of thermal properties by the transient thermoreflectance method," *Components and Packaging Technologies, IEEE Transactions on*, vol. 28, pp. 39 – 44, Mar. 2005.

[85] A. J. Minnich, J. A. Johnson, A. J. Schmidt, K. Esfarjani, M. S. Dresselhaus, K. A. Nelson, and G. Chen, "Thermal conductivity spectroscopy technique to measure phonon mean free paths," *Phys. Rev. Lett.*, vol. 107, p. 095901, Aug. 2011.